GLASS SUBSTRATES FOR MICROFLUIDIC APPLICATIONS

BY

JOSEPH M. DORSHEIMER

A THESIS

SUBMITTED TO THE FACULTY OF
ALFRED UNIVERSITY

IN PARTIAL FULFILLMENT OF THE REQUIREMENTS
FOR THE DEGREE OF

MASTER OF SCIENCE

IN

MATERIALS SCIENCE AND ENGINEERING

ALFRED, NEW YORK

APRIL, 2004

GLASS SUBSTRATES FOR MICROFLUIDIC APPLICATIONS

BY

JOSEPH M. DORSHEIMER

B.S. SUNY BUFFALO (2002)

SIGNATURE OF AUTHOR (Signature on file)

APPROVED BY (Signature on file)
REBECCA DeROSA, ADVISOR

(Signature on file)
JAMES SHELBY, ADVISORY COMMITTEE

(Signature on file)
ALAN GOLDSTEIN, ADVISORY COMMITTEE

(Signature on file)
SUBRUTA SAHA, CHAIR, ORAL THESIS DEFENSE

ACCEPTED BY (Signature on file)
ALASTAIR CORMACK, DEAN,
SCHOOL OF ENGINEERING

Acknowledgements

First, I would like to thank my advisor and committee members, Dr. DeRosa, Dr. Shelby and Dr. Goldstein, for their support during my research. I would also like to acknowledge Dr. Matthew Hall for all of the suggestions that he gave and all of the discussions that we had. Dr. Alexander Fluegel also helped with buffer formulations and electrophoresis experimental setup. Many thanks go to Eric Telfeyan for teaching me to use all the equipment in our labs. Thanks also go to my friends, especially Ashleigh, Michelene, Brian, and the glass crew. Katie and Nicole's efforts are also noted for collecting numerous contact angle measurements.

I would also like to thanks the librarians at Scholes for all of their help, especially Mercedes Hanbach for acquiring so many interlibrary loan items.

Last but not least, thanks to my family for their continued support and love throughout my time here at Alfred. Also, I must thank my fiancée, Amy, for her unwavering support and love.

Table of Contents

List of Tables

List of Figures

Abstract

Various glass compositions, including a soda-lime, float, binary sodium silicate, and phosphate glass, were treated using five aqueous solutions combined with ultraviolet light exposure. The goal of the work was to find a glass substrate that would be suitable for microfluidic applications. In order to be a suitable substrate, the masked channel on the glass surface must be able to support fluid migration when an external potential is applied. Contact angle analysis and grazing angle infrared spectroscopy measurements were the primary tools used in the characterization of the hydrophilic nature of the surfaces. Impedance and electrokinetics were used to test the channel conductivity and fluid flow.

When glass is exposed to aqueous solutions, surface bonds, such as Si-O-Si, are exploited to form a gel layer on the surface. The gel layer possesses a more open structure than the original glass which gives it the ability to support electrical current flow and fluid migration. Contact angle data that was collected suggests that the water plasma treatment that was used to clean the surfaces made them hydrophilic. Low, wetting contact angles were measured on the surface using water. However, infrared spectroscopy did not show activity in the hydroxyl region of the spectra. As the treatments progressed the contact angle increased, suggesting that the surface was becoming less hydrophilic. The hydroxyl groups present on surface are reactive, meaning that any contamination that contacted the surface may have become an adsorbed species thus making the surface more hydrophobic. Again, infrared spectroscopy did not pick up any contamination present on the surface. The fact that neither hydroxyl nor contamination layers were observed can be explained if the incident angle of the infrared light is considered.

Of the compositions that were tested, phosphate glass immersed in Laemmli buffer performed the best in the electrophoresis experiments. The combination represented a moderately non-durable phosphate glass treated and a moderately high pH Laemmli buffer. The success of the phosphate glass and Laemmli buffer treatment could be an effect of the surface charge that resulted from a high pH treatment.

1. Introduction

Microfluidic devices are analytical systems that have been scaled down to a considerably smaller size than traditional laboratory instruments. At the heart of the microfluidic device is one or more channels which are typically less than 500μm in at least one dimension. They are used in many applications, including nano-scale chemical reactions, micro-electro-mechanical systems (MEMS), and separation of biological fluids. Recent discoveries include a glass microchip that supports chemical reactions on the 1nL scale followed by an electrophoretic separation of the amino acid products,[1] a polymer microchip used for electrokinetic fluid pumping[2] and a soda-lime glass microchip used for two-dimensional liquid-phase separations of peptides.[3]

Microfluidics are widely used in lab-on-a-chip technology, which allow multiple steps of a process to be automated and carried out on a small scale with virtually no concern for contamination. With recent advances in the field, the capability of these "miniature laboratories" has grown exponentially. Since market analysis indicates that molecular diagnostics, including microfluidics, will become a 3-5 billion dollar a year industry over the next five years, the ability to inexpensively fabricate devices will be crucial to the success of the field. Continued research is being done to find the best material and fabrication method to make inexpensive, disposable devices. Current microfabrication techniques for the preparation of microfluidic devices include photolithography, chemical etching, laser ablation, ion etching, injection molding and embossing.

1.1. Conventional Formation Techniques

Many of the formation techniques that are currently used to make microfluidic devices have been taken from the semiconductor industry. Each technique has its own drawbacks, which will be discussed in subsequent sections. The selection of microfabrication method is important because they each yield diverse products.

1.1.1. Photolithography

Photolithography is the basis for the methods most commonly used to fabricate microchannels.[4] There are many steps[5] that must be completed in order for a successful product to be manufactured. The photolithography process includes:

- Chemical cleaning to remove impurities
- SiO_2 barrier layer applied to surface
- Application of thin and uniform layer of photoresist
- Removal of solvents used in application of photoresist (soft-baking), making the surface photosensitive
- Application of photo mask
- Exposure to high intensity UV light and development
- Hard-baking, which hardens the photoresist and improves surface bonding

There are two types of photoresist, positive and negative. A depiction of both methods is shown in Figure 1.1. Exposure of positive resist to UV light causes reactions to occur that result in the exposed resist becoming more soluble. Therefore, the exposed section can be washed away during development. The mask used contains an exact copy of what will be seen on the wafer. The negative resist operates in exactly the opposite way. Exposure of negative resist causes it to polymerize, and makes it less soluble. The mask for a negative resist must contain the inverse of the desired pattern.

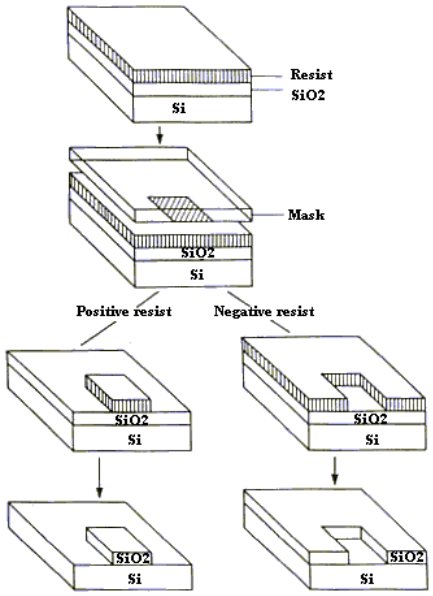

Figure 1.1. Application of positive and negative photoresist and their final products[6]

A cover plate, typically made of glass is applied over the top of the newly formed channel to form a capillary.[7,8] The major problem associated with this method of fabrication is the cost. This technique is expensive and, therefore, any new successful fabrication method that can be done at a lower cost is highly valuable to the furthering the field of microfluidic devices.

1.1.2. Chemical Etching

Chemical etching is used to remove material from a substrate in a selective manner. The depth can be controlled to a few angstroms. The technique is similar to photolithography, that is, a mask is applied, exposed to light, and developed. After the process is complete, the substrate is chemically etched to the desired pattern. Both wet and dry chemical etching techniques are used.

Wet chemical etching is primarily used for cleaning, polishing and resist removal. The chemical reactivity of the etching fluid is affected by both the temperature of the liquid and the amount of agitation.[9,10] In most cases, the etch process is isotropic, i.e. the etching occurs at the same rate for all directions. The most noteworthy exception to this

rule is when silicon is etched using hot potassium hydroxide (KOH) and water mixture; a trapezoidal channel results from the anisotropic etch.[11]

There are many dry etching processes that can be used to form microfluidic channels, including reactive ion etching (RIE), ion beam etching (IBE), and chemical assisted ion-beam etching (CAIBE).[11] RIE relies on the concurrent exposure of the substrate to fluxes of energetic particles and chemical reaction species.[11] Reactive gas or gases are pumped into an evacuated chamber where the reactive ionic species are created using a radio-frequency-induced-plasma. The etching process occurs by a chemical reaction between the substrate and atoms or radicals produced by the plasma; etched materials are pumped away as gaseous species. Dry etching techniques only require small amounts of reactive gases, resulting in smaller amounts of waste, whereas wet etching techniques require great amounts of liquid that must be properly disposed of after use.[5]

1.1.3. Embossing

Hot embossing, or imprinting, techniques were introduced in the late 1990's for use with plastic substrates.[12] The pioneering methods for the embossing technique used a simple wire to create the desired pattern.[13] The process involves a wire being placed on the desired substrate; followed by the pressing of the substrate between two plates at slightly elevated temperatures, depicted in Figure 1.2. This process can also be run at room temperature; however, pressure must be applied to compensate for the reduced temperature. New advances have been made since the first wire imprinting technique was conceived, however, the method is still used today.[14,15]

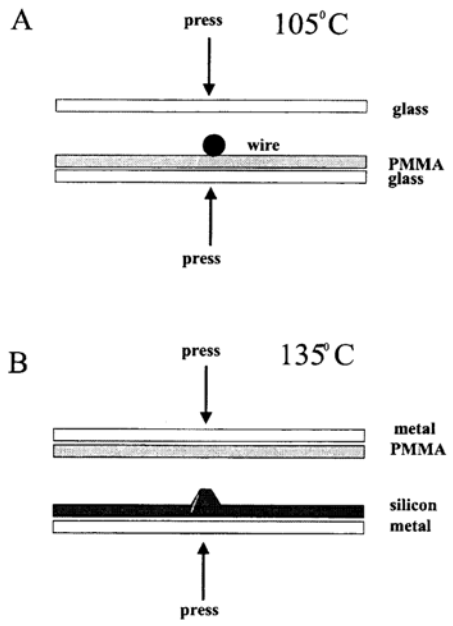

Figure 1.2. (A) Fabrication process for wire-imprinted devices, (B) Fabrication process for silicon-template-imprinted devices[13]

A recently implemented technique for imprinting involves using a silicon stamping tool, seen in Figure 1.2(B).[12] After the design is complete (with the aid of a CAD program), the template is printed onto a transparency that is used as the mask. In a process similar to that of photolithography, the substrate is coated with a masking layer and a photoresist layer is applied. The sample is exposed to UV light and the photoresist is developed. The image is transferred to the masking layer using a chemical etching technique, typically with hydrofluoric acid (HF) or KOH depending on the masking layer composition. After the masking layer has been removed, the exposed silicon is further etched anisotropically which results in channels with trapezoidal geometry. The completed silicon stamp may be used for imprinting at room temperature[16] or an elevated temperature.[13]

1.1.4. New Method

As an alternative to these methods, the current work looks to expand on a novel fabrication method for microfluidic channels using glass and aqueous solutions. When glass samples are exposed to aqueous solutions under the right conditions, the result is a modified surface layer. The modification of the surface, also termed corrosion or

degradation, can yield a gel layer which has properties much different than that of the bulk glass. From previous work,[17,18] it was shown that the gel layer can support current flow and electrokinetic fluid transport under an applied voltage.

1.2. Properties of Materials

The materials play an important role in the fabrication and functionality of the devices. When microfluidics were introduced in the 1990's, glass was used as the primary substrate.[12] However, recent material advances and cost concerns have introduced polymers into the microfluidics field. In microfluidic applications, properties of the material that may be of fundamental importance include machinability, surface charge, molecular adsorption, electroosmotic flow mobility, and optical properties.[12]

Recently, polymers have received much attention as a substrate for microfluidic devices at the expense of fused silica and other glasses. Polymer devices have advantages over their glass counterparts, including inert surface characteristics, possibility of high resolution fabrication of deep and shallow features with well-defined vertical walls, certain chemical resistance, low fabrication temperatures, mass production ability and cost.[19] Polymers such as poly(methyl methacrylate) (PMMA) and poly(dimethylsiloxane) (PDMS) among others, have been utilized as substrates for microfluidic systems.[13,20-22]

As previously mentioned, the present study investigated the formation of glass microfluidic channels using a novel fabrication method. Bulk glass and surfaces have vastly different properties and the current work aims at exploiting the corrosion behavior of glass. The process of forming glass forces the surface to be different than the bulk. In the bulk of the glass, all of the bonds are satisfied and there are few, if any, strained areas in the network. The surface structure of glass is more strained due to the abrupt termination of the network. The surface is also different because it is in contact with the environment in which it is formed. This results in the formation of strained structures on the surface, causing the surface to be more reactive and more easily manipulated. When stressed bonds are attacked, they preferentially break to decrease the systems overall energy.

1.2.1. Glass Durability and Corrosion

1.2.1.1. Aqueous Glass Durability

When glass is added to an aqueous solution, the glass surface undergoes chemical and structural changes.[23] The following processes can occur when liquid water comes in contact with glass:[24] dissolution, ion-exchange, hydration, formation of a reaction product layer on the surface and hydrolysis. Aqueous durability of a glass is controlled by many factors, including but not limited to, glass composition, temperature, pressure, length of exposure, and the ratio of the exposed glass surface area to the volume of solution.[25] The extent of the reaction is also significantly controlled by the amount of products that accumulate in solution. Glass durability is a major concern for all of the glass industry; typically research is done to promote increased durability of a glass. The current work has considered glasses based on durability, or the lack thereof. The glass required for the study must be durable enough such that the network forming bonds are strong enough to hold together, even in the presence of a very loosely bound gel layer.

It has been suggested that the reaction in the presence of an aqueous solution occurs in two stages.[25,26] The occurrence of each stage can be related to the pH of the solution. Typically, the first stage will occur in acidic pH ranges and the second will occur in basic pH ranges. The first stage involves the ion exchange of alkali ions from the glass and hydrogen ions from the solution. The glass is made susceptible to an attack by water through the diffusion of alkali ions. The vacant sites left by the alkali can either be filled in by hydrogen ions via ion-exchange or by other alkali ions that diffuse through the bulk glass to the surface.[27] The hydrogen ions have the same ionic charge as the sodium ions, however, their ionic radius is smaller. The size difference results in an overall weaker glass network. The silica network is primarily undisturbed during the first stage, and therefore, a silica-rich layer is formed.[28] The result of the stage one reactions is the formation of a gel layer on the surface. We intend to take advantage of stage one reactions to modify the surface layers of the glass. The alkali ions leached from the glass in the first stage undergo ion exchange with the hydronium ions or water molecules in the aqueous solution, increasing the pH and allowing a second type of reaction to occur at the surface. The second stage of the reaction is characterized by the dissolution of the silica

network in the glass. Typically, this will occur once the pH has been elevated. If the stage two reactions continue, the silica-rich surface layers formed during stage one will dissolve into solution.

1.2.1.2. Silicate Glass Corrosion

The silicate glass network can be visualized as interconnected Si-O-Si ring structures, containing a varying number of Si atoms (typically between 2 and 6). The rings with the least stress are the ones that contain a higher number of Si atoms; a 6 member ring is the most stable. The most strained configuration possible is an edge-shared tetrahedra, or two member, structure.[29] The bulk glass is full of high Si rings which provide stability, whereas the surface contains many low Si atom ring structures along with non-bridging and dangling oxygen atoms which are more reactive than Si-O-Si linkages.

The Si-O-Si linkages will react with water to form silanol groups (Si-OH) via reaction (1).[28]

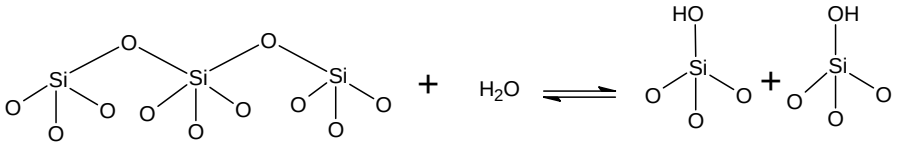

(1)

The result of reaction (1) is the formation of a hydrated gel layer that has a significantly lower surface energy than the initial glass surface. On top of the chemisorbed species, physical adsorption of water can occur, as seen in Figure 1.3. Physisorption does not break bonds in the glass, instead water molecules become hydrogen bonded to the hydroxyl groups produced via reaction (1).

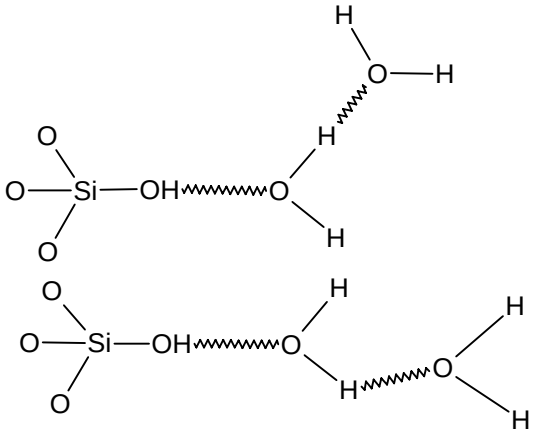

Figure 1.3. Physical absorption of water molecules on top of chemisorbed species

As noted above, reaction (1) is reversible. The glass can be dehydroxylated by placing it into an environment with an elevated temperature or significantly decreased humidity. The dehydroxylation of glass will occur at different temperatures depending on the stability of the ring structure that was broken. If the original ring structure was relatively stable, the dehydroxylation will occur at lower temperatures returning the glass to its original state. If the initial ring structure was highly stressed, a higher temperature is required to drive off the remaining OH groups and reform the Si-O-Si linkages. This is important to mention because the gel layer on the surface can be destroyed if it is placed in harsh environments. Previous aging studies[30] have shown that the gel layer can remain on the surface for a significant amount of time when exposed to normal room temperature and humidity.

1.2.1.3. Phosphate Glass Corrosion

Both silicate and phosphate glasses behave in a similar manner when exposed to aqueous environments. Studies have shown that phosphate glasses contain polymeric structures that are controlled by the composition of the glass.[31] The repeating unit of the glass is PO_4^{3-}, which can be attached to three neighboring groups to yield P_2O_5. The P-O-P bond is not thermodynamically stable and the hydration reaction (2) is favored.

$$\text{P-O-P} + H_2O \leftrightarrow 2\ \text{P-OH} \qquad (2)$$

Most phosphate glasses have poor durability, making them unfit for many applications.[32] However, since we want to take advantage of the susceptibility of the glass to corrode, phosphate glasses were studied in this work.

1.3. Transport Phenomena

Since the material introduced into the channel must travel, fluid transport plays a big role in the functioning of the devices. Electrokinetics is the most common transport mechanism for microfluidic devices. Two principal electrokinetic processes of interest for microfluidics are electroosmotic flow for solution layers or electrophoretic flow for molecular transfer.[33]

Electrophoresis is defined as the movement of charged particles suspended in a liquid through a medium, under the influence of an applied electric field.[34] Success is defined as the quality of the fluid migration and separation that can be achieved. Electrophoresis requires the application of a potential gradient to the media, which can take on many forms. Typically, separation during electrophoresis occurs based on charge.[35]

Electroosmotic flow (EOF) is described as the movement of an aqueous solution past a stationary solid phase due to an externally applied electric field. EOF is the bulk flow that results from the accumulation of positively charged ions on the channel surface. In our system, the positively charged ions are attracted to the negative ions, mainly SiO_2^-, that are present on the glass surface. The concentration of positive charges on the surface creates a movement towards the negative electrode that drags the entire solution with it, including neutral species. In the case of bare silica, a high pH results in zero protonation of the SiO_2 groups (they are all negatively charged), which results in high EOF toward the negative electrode. When the pH is low, the SiO_2 groups become protonated, yielding a more neutral surface, and the EOF decreases.

Electroosmotic flow is generated and controlled through the solution filled channels via an external power supply. In a system that has a uniform wall charge, EOF produces a plug flow profile (except for a very thin Debye layer to satisfy the no-slip condition), unlike pressure driven flow which produces a parabolic flow profile. The flat

profile allows for the band broadening of "separation plugs" such that the separation fronts do not become dispersed and difficult to see. It significantly affects the separation resolution that a channel can produce. However, if the wall charge becomes variable, as in many microfluidic systems, a pressure flow component is introduced thereby distorting the flow profile. There are many causes for a variable wall charge to exist, mainly analyte molecules absorbed onto the wall surface,[36] imperfections in the fabrication process,[37] or the wall may be designed in such a way to promote disordered mixing.

In microfluidic applications, it is generally desirable to have only one type of flow and not both occurring in the system. The type of flow will be determined, in part, by the charge on the material that is injected to the channel and the surface charge on the substrate. If the species are negatively charged, they will tend to move from the cathode to the anode when a potential is applied in electrophoretic applications. The opposite can be said for a positively charged species. If electrophoretic and electroosmotic flow occur in a given system, instead of separation or uni-directional migration, bi-directional flow will occur and the sample will be spread out along the length of the channel.

One issue with the electrokinetic movement of fluid is that the ions with higher mobility will tend to move through the channel first. The mobility must be considered during an electrophoresis experiment, which typically separates based on size.
Another concern with fluid separation is the complexity of the analyte. Two-dimensional electrophoresis (2DE) is a technique that is commonly used for biological separations, since a one dimensional system will not suffice. When 2DE technology is coupled with a detection scheme, such as laser induced fluorescence or mass spectrometry,[19] it becomes an even more powerful tool for biological analysis. As its name implies, 2DE separates using two dimensions or channels that are orientated at right angles. A typical experiment would first separate the species based on their isoelectric points followed by a molecular weight separation. The two dimensions allow for separation over a larger area which typically yields increased resolution.

1.4. Current Technology of Microfluidics

Miniaturization of traditional laboratory instrumentation has many advantages, including improved performance, speed and throughput, and reduced costs due to lower chemical consumption.[19] The lab-on-a-chip, or micro-total analysis system (μ-TAS), has been the driving force for miniaturization. The small systems can include such operations as sampling, sample pretreatment, mixing, separation, and detection[20] and are used for many purposes, from DNA sequencing and proteomics to drug discovery.

As expected, the fluid transport properties of microchip-based systems are crucial to the operation of the system. Electrophoresis is the primary technique used for separation using chip based devices, including microfluidics. There are many variations of electrophoresis; however, zone electrophoresis has been the most attractive method for performing such separations due to its simplicity. A potential is applied to a channel that is filled with a buffer solution; the potential allows for sample injection and separation.[38]

More recently, capillary electrophoresis (CE) has been used as the principle analytical technique for the devices, allowing the flow of liquids to be controlled by an electric field rather than by pumps and valves.[20] Injection ports allow for the introduction of the sample and buffer solutions so that all steps can be automated. Both the sample and the buffer are electrokinetically transported to a mixing junction, where a high voltage is applied and a potential is present to carry the fluid down the separation channel. The first CE devices contained a single, straight separation channel that was patterned on a relatively large substrate.[39] As time progressed, the substrate was miniaturized and the separation channel began to take on different geometries. Jacobson et al[40] tested the feasibility and efficiency of a serpentine shaped channel. The serpentine geometry allowed the dimensions of the device to shrink, while not comprising the separation length. They found that while the serpentine channel structure exhibited band-broadening phenomena, it was not a severe problem in any of their experiments.

1.5. Current Work

As an alternative to the fabrication techniques presented, a novel fabrication method for creating microfluidic channels has been tested. The current investigation utilized glass corrosion in aqueous environments to create a gel layer on the substrate surface. The aqueous environments included de-ionized water and several buffer solutions to see how the presence of ions in solution affects the glass. Each substrate composition was monitored using contact angle analysis, Fourier transform infrared spectroscopy (FTIR), and electrochemical impedance spectroscopy.

2. Experimental Procedure

2.1. Materials

2.1.1. Glass Compositions

Glass compositions of varying durability were considered for our investigation. The different compositions are in Table 2-1. Corning Inc. microscope slides (number 2947) were used or the soda-lime silicate (SLS) substrates. The dimensions of the slides were 76.2x25.4x1mm. The float glass was a generic composition, with average dimensions of 40x25x5.75mm, cut from a large plate. The process of making float glass yields very different properties for each side. The air side of the float glass was used, since the tin side has greater durability. The two binary sodium silicates were formulated by PQ Corporation. The as-received form was unworkable for the desired use so the pieces were melted in a platinum crucible to form a workable shape. The binary sodium silicate pieces were cut and polished using water and a circular sander with SiC paper with the following grit: 180, 240, 320, 400, 600, 800, and 1200. The phosphate glass (LG-770) was obtained from Schott Glass Inc. For each treatment within each composition, two replicates were tested.

Table I. Glass Compositions Used in the Current Study

	Float Glass	Corning SLS	Sodium Silicate (PQ 2.0)	Sodium Silicate (PQ 3.2)	Phosphate (LG-770)
SiO_2	73.1	73	67	76	-
Na_2O	13.7	14	33	24	-
CaO	8.9	7	-	-	-
MgO	3.8	4	-	-	30 (+K_2O)
Al_2O_3	0.1	2	-	-	10 (+Nd_2O_3)
K_2O	0.1	0	-	-	30 (+MgO)
P_2O_5	0.1	0	-	-	60

2.1.2. Aqueous Solutions, Gels and Dyes

Glass samples were treated with the following solutions: distilled water, 1x Laemmli running buffer, 0.3M K-Phosphate buffer with a pH of 5.8, and three volume percent polyethylene glycol (PEG) 400 added to the latter two buffer solutions. The 5x stock Laemmli buffer was formulated by adding 72g glycine (J.T. Baker, ultrapure 99.8%) and 14.5g tris (Fisher, molecular biology grade) to 1 liter of distilled water. Three volume percent PEG 400 (Union Carbide) was added to the 1x Laemmli buffer. Stock solutions of potassium phosphate monobasic (KH_2PO_4, Fisher, certified A.C.S. 99.7%) and potassium phosphate dibasic (K_2HPO_4, Fisher, certified A.C.S. 99.88%) were made by adding 1 mole of solute to 1 liter of distilled water. The 0.3M K-phosphate buffer was made by combining 25.5mL K_2HPO_4, 274.5mL KH_2PO_4, and 700mL of distilled water. Three volume percent PEG 400 was added to 0.3M K-phosphate buffer. An agarose gel (Fisher, molecular biology grade) was used to connect the buffer reservoirs and the glass sample. A solution of bromophenol blue (bpb) tracer dye, diluted in deionized water, was used during the electrophoresis to measure the fluid migration. A bovine hemoglobin protein (Aldrich, lyophilized) was also used for migration tests, and was diluted to 1mg/mL in deionized water. A 50:50 volume mixture of hemoglobin and bromophenol blue was also used for migration tests. All chemicals were used as-received.

2.2. Procedures

2.2.1. Sample Preparation and Exposure

Plasma treatments are commonly used to clean glass surfaces. The process removes unwanted organic and metal oxide groups from the surface. The plasma treatment forces the alkali ions near the surface to migrate since ions are approaching the glass.[41-44] The mobile alkali ions in the glass are repelled from the surface and move

deeper into the glass.[45] The water plasma treatment is also an ideal method for creating a hydrophilic surface, which is enhanced by hydroxyl groups added to the immediate surface region.[46]

The plasma treatment was carried out using an LF-5 system (Mercator Control Systems, Inc.). The chamber was vacuum pumped (Duo Seal Vacuum Pump, The Welch Scientific Company) down to 0.10-0.20 Torr. The gaseous water flow was adjusted such that the pressure in the chamber equilibrated to 0.75-0.85 Torr. The radio frequency was set to 50 Watts and the each treatment lasted seven minutes.

The samples were exposed to UV radiation in one of two different chamber environments. For some samples, a Q-SUN/1000 xenon test chamber was used with an exposure wavelength of 340 nm and an irradiance of 0.80 W/m^2. The Q-SUN chamber was connected to a distilled water source and water was pumped at 0.3 liters per minute into the chamber to counter the evaporation that occurred. Also, a Macam flexicure system equipped with two 8mm liquid light guides was used. The UV source was a Philips medium pressure metal halide lamp (HPA 400/30S) with a wavelength range between 320nm and 380nm. The solution was changed daily to prevent the buildup of reaction products.

2.2.2. Contact Angle Measurements

Contact angle measurements were used to monitor the glass surface hydration. Contact angle measurements were taken in 24 hour increments of exposure for each sample. Sessile drop measurements were taken at room temperature and atmospheric conditions using a Tantec contact angle meter. The Tantec Cam-Micro model consists of a 22 gauge blunt needle from which a drop was manually applied to the sample and a goniometer grid is used to measure the size of the sessile drop.

Once the sample was removed from its Petri dish, it was rinsed with ultra pure water, dried using an optical grade cloth and placed on the stage. A droplet of ultra pure water, with an approximate width of 10 divisions on the goniometer grid, was formed. The stage was raised until the droplet of water was transferred to the surface of the glass and the contact angle was recorded. After the angle was recorded, each drop was wiped

off the surface using an optical grade cloth and the process was repeated. Ten measurements were taken to ensure that an accurate average could be reported.

2.2.3. Fourier Transform Infrared Spectroscopy Measurements

Infrared spectroscopy is a technique that has many uses in materials characterization, including the identification of species that are present on the surface of a material. When infrared light strikes a material, the material can reflect, transmit or absorb the radiation. When the light strikes the surface at a low angle, or grazing angle, information about the surface of the material can be determined. Fourier transform infrared spectroscopy uses an interferometer to modulate the intensity each wavelength of light. The beam is sent to a beam splitter, which divides the light into two optical path lengths, and the recombination allows for constructive and deconstructive interference to occur.

Infrared spectroscopy measurements were taken in 24 hour increments of exposure for each sample. A Bruker Vector 22 spectrometer was used with an advanced grazing angle (AGA) accessory manufactured by Pike Technologies, Inc; Figure 2.1 is a schematic of the accessory. The IR light enters the accessory through (A), reflects off of the pin mirror (B), strikes the sample (C) at an angle of 80º from the surface normal, passes through the prism (D) which redirects the light to the detector (E).

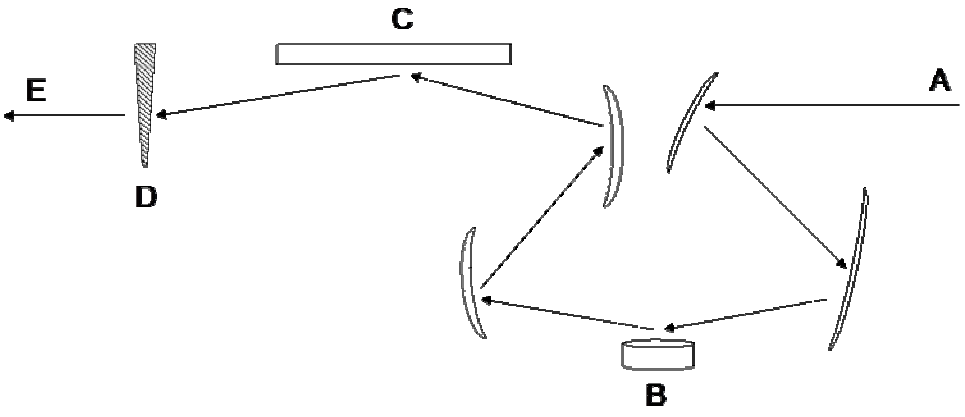

Figure 2.1. Schematic of advanced grazing angle accessory

The accessory allowed for infrared light to strike the surface at an incident angle of 80º from the normal, resulting in a measurement that reflected the properties of the near surface region. The spectrometer was equipped with a liquid nitrogen cooled mercury cadmium telluride (MCT) detector. Each spectrum was taken as an average of 1000 scans over a frequency range of 4000-575cm^{-1}. All spectra were taken in Kubelka Munck units, which are defined as "$(1-R)^2/2R$ where $R=R_{sample}/R_{reference}$ is the sample reflectance measured relative to the reference standard"[47] and is very similar to log (1/R). A dry nitrogen (N_2) purge, at a flow rate of 55 mL/min, was used to eliminate signal from the ambient environment. OPUS-NT software was used for the baseline corrections and smoothing functions.

2.2.4. X-Ray Photoelectron Spectroscopy Measurements

X-ray photoelectron spectroscopy (XPS) is a tool that is used for elemental analysis (except hydrogen and helium) of surfaces and concentration profiles of near-surface areas. The technique is based on two phenomena, the photoelectric effect, outlined by Einstein in 1905, and radiationless transition, that was discovered in 1923.[48] If an incident x-ray photon has sufficient energy, it ejects a core shell electron, producing a photoelectron. The technique is very surface sensitive because the emitted photoelectrons possess low kinetic energies. If an emitted electron takes part in an inelastic collision, the probability is high that it will no longer possess enough energy exit the material. A concentric hemispherical analyzer (CHA) is used to determine the energy of each of the photoelectrons and yields a spectrum with different photoelectron peaks; the binding energy of each peak is element specific. The peak area can be used to find the composition and the elemental depth profile of the material.

With help from the Materials Characterization Laboratory at Penn State University, XPS data was obtained using a Kratos Analytical axis ultra. The x-ray source was monochromatic aluminum (1486.6eV) with 280 watts of power and a 4keV Ar^+ ion beam was used with a sputter rate of 1.3Å/sec. The samples were wrapped in aluminum foil and mounted on conducting carbon tape; a spot size of 110μm was used. All experiments were performed in ultra high vacuum (UHV). A photograph of the

equipment can be seen in Figure 2.2; important components include: CHA (A), monochromator (B), x-ray source (C), sample positioning device (D), sample chamber (E), and detector (F).

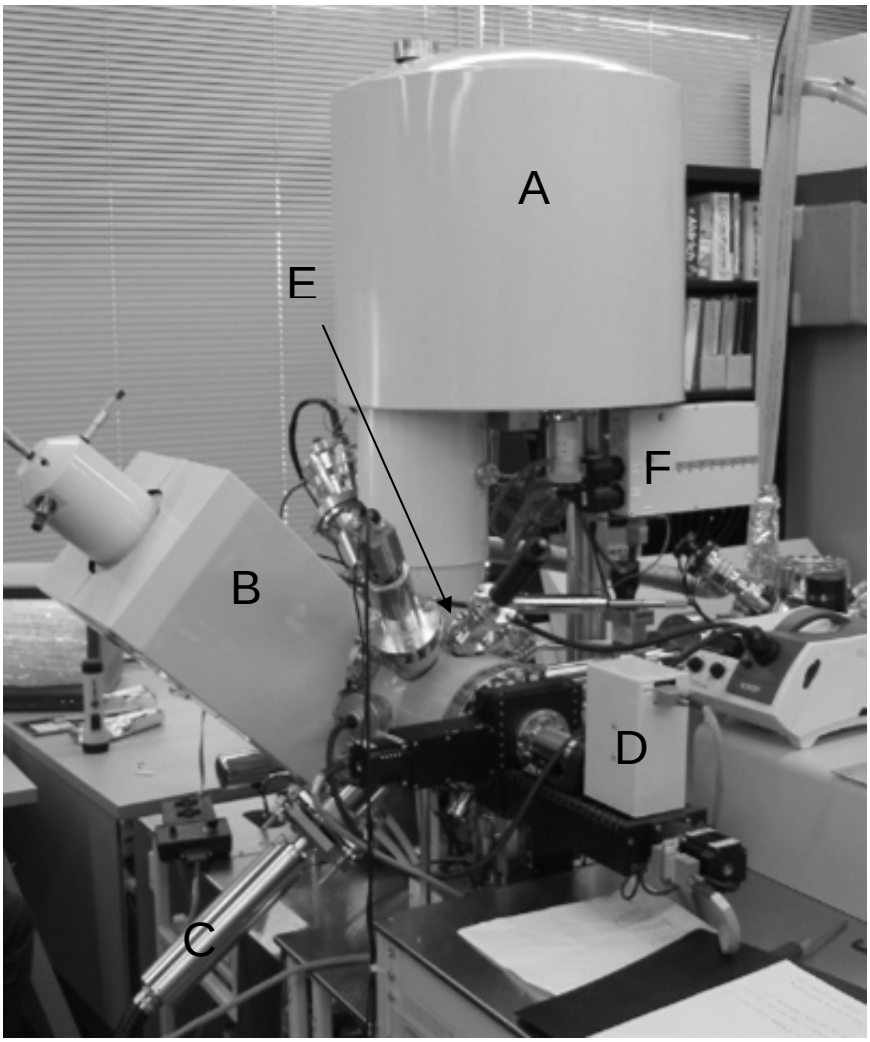

Figure 2.2. Photograph of the Kratos Analytical axis ultra XPS equipment

2.2.5. Electrochemical Impedance Spectroscopy Measurements

Electrochemical impedance spectroscopy (EIS) is widely used for the characterization of coatings and thin films applied to surfaces because of its non-destructive nature. An important advantage to the technique is the small amplitude signals, typically 50-100mV, that are required as input. The low amount of input signal ensures that the properties being measured are not disturbed. AC methods are becoming

more prevalent in research due to their small perturbation signals and the ability to test low conductivity materials.[49] In many materials, the impedance will vary as the frequency of the applied voltage changes. This variation has to do with the properties of the material, including physical structure and chemical processes occurring in it. Our setup used a three electrode system consisting of a working, counter and reference electrode. Measurement of the potential between the working and reference electrodes allows for the change in potential of the working electrode needed to cause current flow.[49]

Impedance spectroscopy measurements were taken in 24 hour increments and used to monitor the progress of the surface conductivity. After the glass samples were placed in the minicell (model EC370M, E-C Apparatus Corporation), agarose was applied to connect the glass to the reservoirs, seen in Figure 2.3 and an impedance/gain phase analyzer (Solartron model 1260) and a potentiostat (Solartron model 1287) were connected to the cell via the three electrodes. A platinum counter electrode and a reference electrode (SCE) were attached to the cell in a manner shown below. The impedance was measured as the frequency was swept from $1x10^5$-0.1Hz with an applied AC voltage of 100mV.

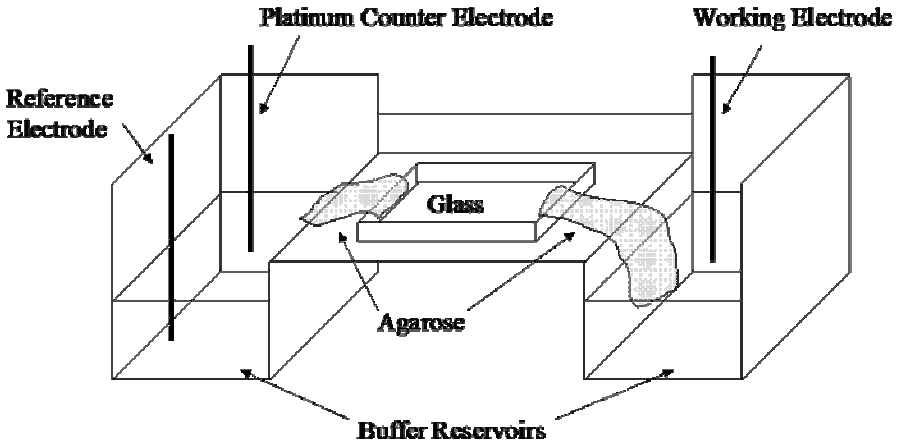

Figure 2.3. Schematic of impedance spectroscopy experimental setup

Figure 2.4 shows the Bode plots for the aqueous solutions, which were obtained by submerging all three electrodes into the solution and Figure 2.5 contains the plots for an open and connected circuit.

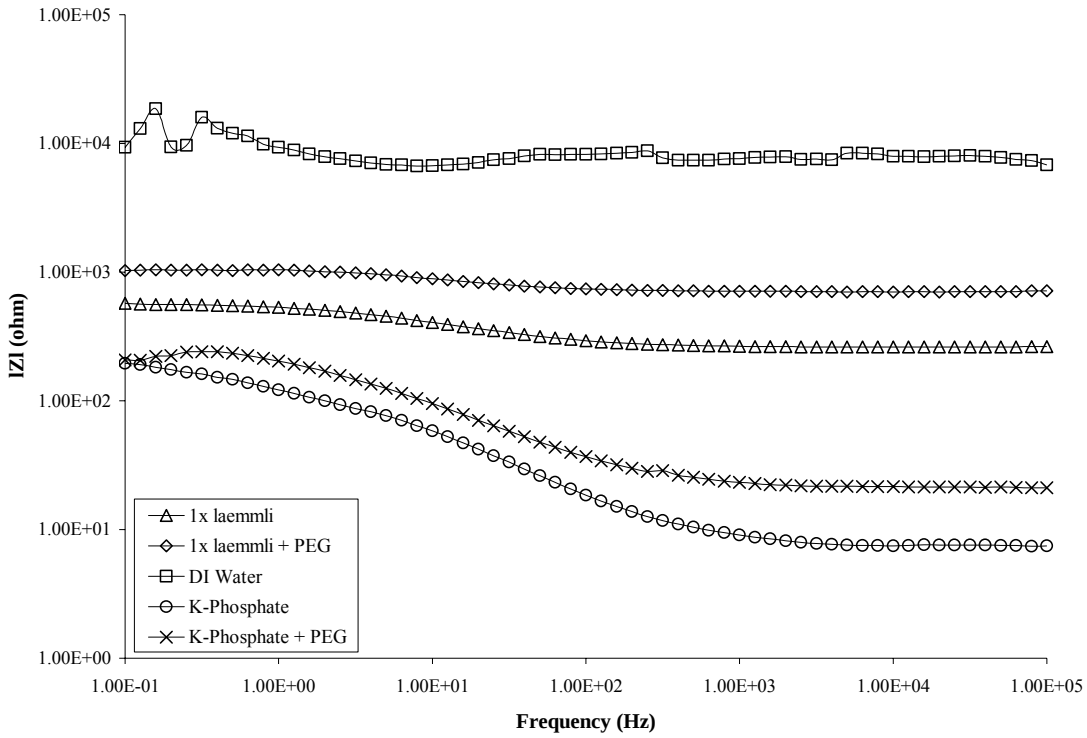

Figure 2.4. Bode plots for aqueous solutions used for treatment

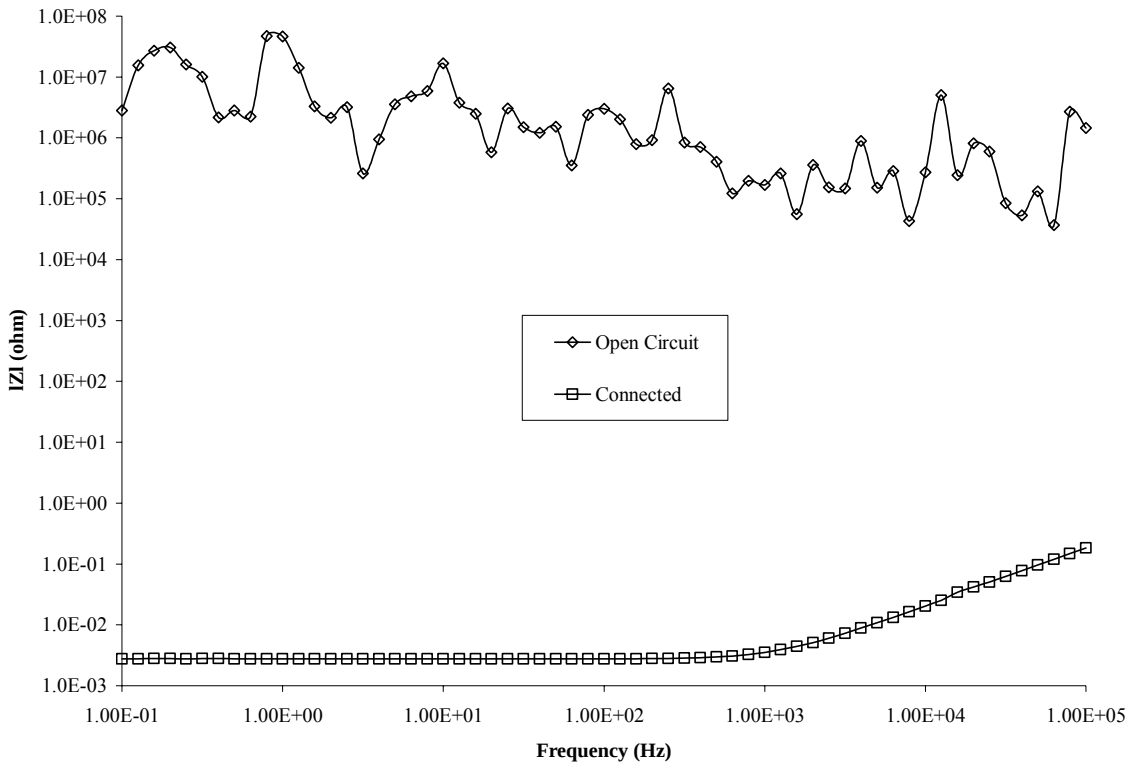

Figure 2.5. Bode plots for an open air circuit and a circuit formed by connecting electrodes

2.2.6. Electrophoresis Experiments

The glass samples were placed into the same minicell described above, and the power supply (E-C Apparatus Corporation) was connected through a standard voltmeter. The mini cell can be seen in Figure 2.6. Each glass sample was rinsed with the exposure solution and allowed to air dry for 5 minutes before being placed into the minicell. Bromophenol blue tracer dye was placed in the center of the channel and a microscope slide was placed on the agarose to prevent the dye from prematurely drying out. A drop size of 1μL was found to be the most reproducible drop size that could be dispensed with the micropipettes. The power supply was set to 200V and the DC current through the glass channel was measured using a standard voltmeter.

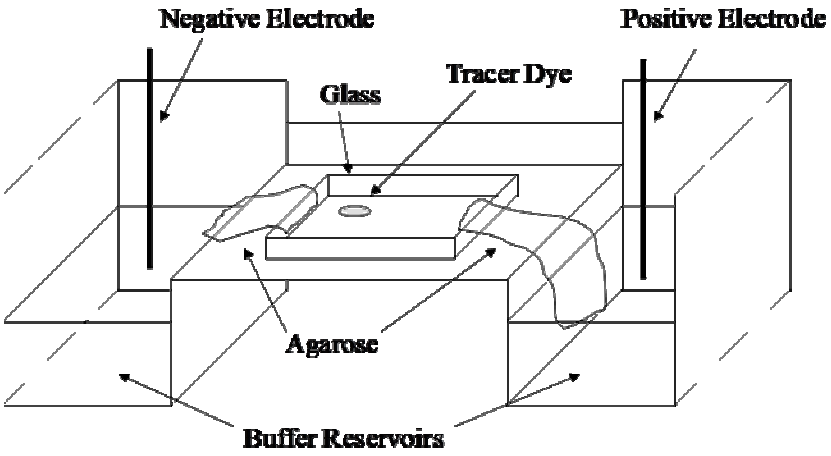

Figure 2.6. Schematic of electrophoresis experimental setup

3. Results

3.1. Soda-Lime Silicate

3.1.1. Contact Angle Analysis

A summary of the contact angle as a function of treatment time can be seen in Table II. The as-received soda-lime glass displayed a mild hydrophobic character, with contact angles in the mid 30's and 40's. After a plasma treatment, the angles sharply decreased to values near zero. The contact angles after increasing treatment times are also included.

Table II. Contact Angle Measurements for Soda-Lime Glass

Treatment Solution	As-Rec'd	After Plasma	24 hour	72 hour	120 hour
DI Water	32.3º ± 4.9	0.0º ± 0.0	18.5º ± 1.8	18.5º ± 2.1	17.7º ± 1.9
1x Laemmli Buffer	45.2º ± 3.3	4.5º ± 2.1	18.6º ± 6.5	27.9º ± 7.8	31.1º ± 11.4
K-Phosphate Buffer	38.6º ± 3.9	1.8º ± 1.1	14.3º ± 2.7	13.3º ± 2.3	13.5º ± 2.6
K-Phosphate Buffer plus PEG	32.1º ± 5.6	1.4º ± 0.7	19.8º ± 5.3	27.6º ± 6.5	29.1º ± 3.6

3.1.2. XPS

A limited investigation was completed measuring the depletion of sodium ions from the surface of the glass for SLS glass only. The depletion of sodium can be seen as a direct result of the hydration reactions/ion exchange during corrosion occurring at the surface of the glass. When quantified, the gel layer thickness could be determined. The bulk was composed of 13.7% sodium and the depleted surface layer was defined as a sodium concentration less than 5.0%. Depletion depths for samples of soda-lime glass exposed to various conditions are listed in Table III.

Table III. Results from XPS Investigation of Treated Soda-Lime Glass

Treatment	Depletion depth (Å)
As-received	700
Water plasma cleaned	750-850
Water plasma cleaned, immersed in DI water and exposed to UV light	850-950
Water plasma cleaned, immersed in 1x Laemmli buffer and exposed to UV light	650

The data obtained from this limited study are not conclusive and cannot be used in a quantitative sense. However, qualitatively the data can be used to give a general idea as to the thickness of the depleted layer. SLS is considered to be the most durable glass composition chosen for the study, so a depth of 900Å was used for the current per cross sectional area calculations. From the data, the plasma treatment apparently drives the sodium ions further into the glass. This is in agreement with references found in literature.[41,43,44,45]

3.1.3. FTIR

It has been shown in previous work[30] that grazing angle infrared spectroscopy is a viable technique to measure water that is present on surfaces. The same work also detailed the observed peaks for silicate glass and the species responsible for them. For this reason, FTIR data will not be the focus, but instead, used as reinforcement to the other data. Structural changes that occur during hydration will not be discussed in great depth and you are referred to reference 30 and the references therein for that information.

The infrared spectrum undergoes significant changes as the gel layer is formed on the surface of the glass. Specifically, the addition of hydroxyl groups to the surface becomes very apparent between 3600-3000cm^{-1}, where peaks formed as immersion time increased for the soda-lime glasses. Figure 3.1 is an example of the reflection spectra taken of the soda-lime surface as a function of time. The peak at 3260cm^{-1}, which is featured in the zoom pane, is a result of water molecules that are hydrogen bonded to the

Si-OH groups formed on the surface. A special note should be made regarding the large "peak" observed between 1500cm^{-1} and 1000cm^{-1}. It is not a result of the glass samples; it is an artifact of the grazing angle technique that is caused by the change in polarization of the infrared light.

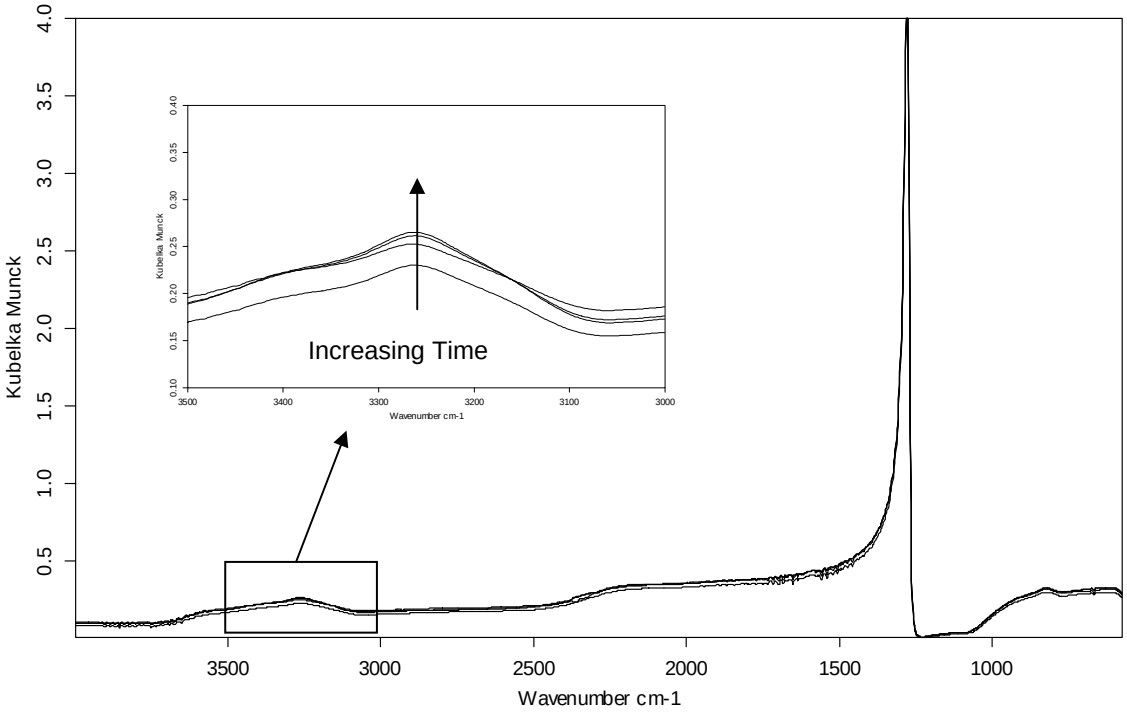

Figure 3.1. FTIR spectra as a function of time of soda-lime glass immersed in Laemmli buffer

Figure 3.2 shows the as-received glass did not have significant activity in the hydroxyl region of the IR spectrum. As the glass samples were treated for a total of 120 hours, each developed peaks within the hydroxyl region. The shoulder observed at 3410cm^{-1} and the peak at 3260cm^{-1} are indicative of silanol groups and molecular water, respectively.

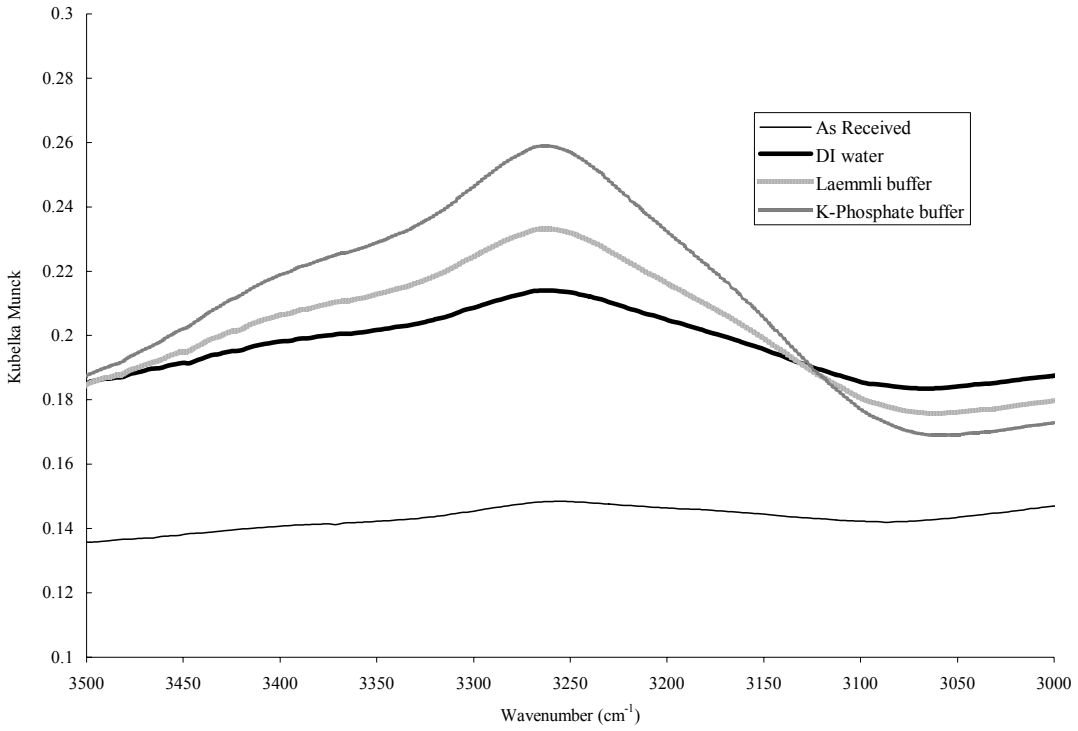

Figure 3.2. FTIR spectra of as-received soda-lime silicate samples immersed in DI water, Laemmli buffer, and K-Phosphate buffer for 120 hours.

3.1.4. EIS

The impedance data for the SLS glass did not show significant change as the treatment progressed. The Bode plot seen in Figure 3.3 is from an SLS sample treated with K-phosphate buffer as a function of treatment time. The noise seen in the low frequency range was observed for nearly all of the glass compositions. One possible explanation for the noise is the high resistive nature of the glass surfaces. At low frequencies, the impedance through the glass channel is extremely frequency dependent. The noise may also be caused by the current choosing the path of least resistance and arcing from one electrode to the other. If the resistance of the ambient environment is less than the glass, this would occur. Experimental data shows that this idea may not be true. If the current was effectively arcing over the glass, the impedance spectra should resemble the impedance spectra seen for an open circuit, presented in Figure 2.5. The noise seen in the glass is similar to the open circuit noise; however the scale of |Z| is three orders of magnitude larger with the glass.

It was originally thought that as the treatment progressed, the impedance would constantly decrease to a lower limit being the condition where solution was placed in the channel and the impedance measured (the SLS buffer line in Figure 3.3). It was also thought that channels with low impedance would support the greatest fluid migration. Following this idea, the impedance for the sample shown in Figure 3.3 would predict that the electrophoresis would not be successful. However, the Bode plot seen in Figure 3.3 corresponds to the electrophoresis photographs in Figure 3.5, showing that fluid migration was achieved.

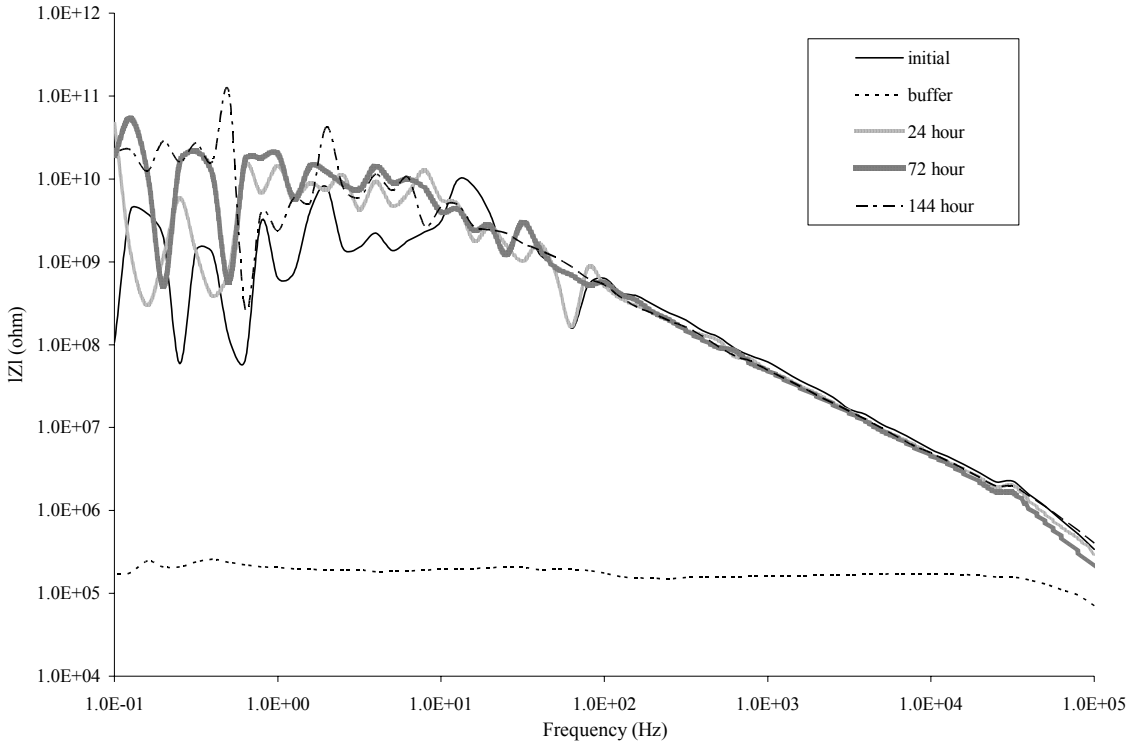

Figure 3.3. Bode plots for SLS glass treated with K-Phosphate buffer at various treatment times.

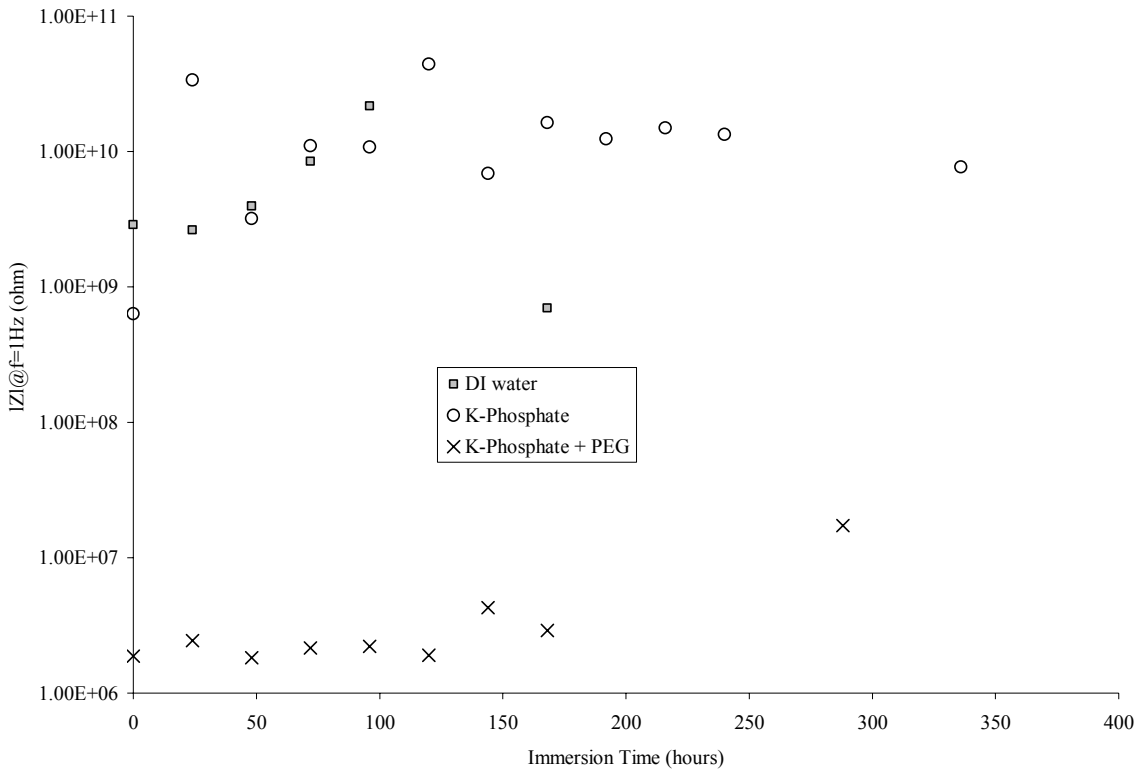

Figure 3.4. Average impedance at 1Hz for SLS glass as a function of treatment time.

3.1.5. Electrophoresis

The SLS glass did not yield satisfactory results during the electrophoresis experiments. More than half of the samples tested did not support current flow, indicated by a reading of 0.000mA measured by a standard voltammeter. The current measurements for the samples that supported flow were generally low, between 0.001-0.007mA and were close to the voltammeter's limit of detection, 0.001mA. A sample that exhibited good current flow and visible dye migration is shown in Figure 3.5. The current per cross sectional area (I/A) for the glass shown in Figure 3.5 was 49.97mA/mm^2.

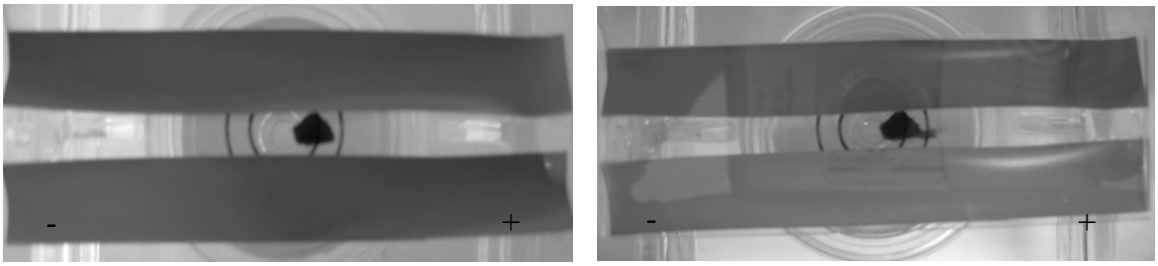

Figure 3.5. SLS glass treated for 336 hours in K-Phosphate buffer at t=0 (left) and t=10 minutes (right) with a 200V applied potential and 1μL drop of bpb. Current per cross sectional area was 49.97 mA/mm^2.

3.2. Float Glass

3.2.1. Contact Angle Analysis

Table IV shows the time dependence of the contact angle for the air side of the float glass composition. The as-received float glass also displayed a mild hydrophobic character, similar to the SLS composition. The plasma treated contact angle is significantly higher in float glass than the other glass compositions.

Table IV. Contact Angle Measurements for Float Glass

Treatment Solution	As-Rec'd	After Plasma	24 hour	48 hour	168 hour
DI Water	32.8º ± 2.9	17.1º ± 2.2	31.1º ± 13.6	20.5º ± 6.9	26.4º ± 5.0
1x Laemmli Buffer		12.4º ± 3.3	17.5º ± 3.3	18.4º ± 3.8	19.0º ± 4.7
1x Laemmli Buffer plus PEG		12.1º ± 1.7	10.9º ± 3.7	11.3º ± 3.8	9.2º ± 1.7
K-Phosphate Buffer		12.2º ± 2.1	26.0º ± 17.0	12.2º ± 2.4	22.5º ± 4.5
K-Phosphate Buffer plus PEG		13.7º ± 1.3	9.7 ± 1.3	9.5º ± 2.6	7.9º ± 1.6

3.2.2. FTIR

The IR spectra for treated float glass can be seen in Figure 3.6 and Figure 3.7. Each of the two figures have been baseline corrected to account for variations in the intensity of each signal and smoothed to remove the small noise. Figure 3.6 shows the glass treated with Laemmli buffer + PEG as a function of treatment time. It is important

to note that the as-received glass did not exhibit significant activity in the hydroxyl region, and that as the glass is treated the peak grows relative to the baseline for each measurement.

Figure 3.7 shows the final spectra collected for float glass treated with DI water, Laemmli buffer and K-Phosphate buffer for 216 hours. When compared to the as-received glass, it can be clearly seen that each treatment modified the surface via the addition of water. Also, there does not seem to be a strong dependence on treatment solution as the 3 solutions produced nearly the same result.

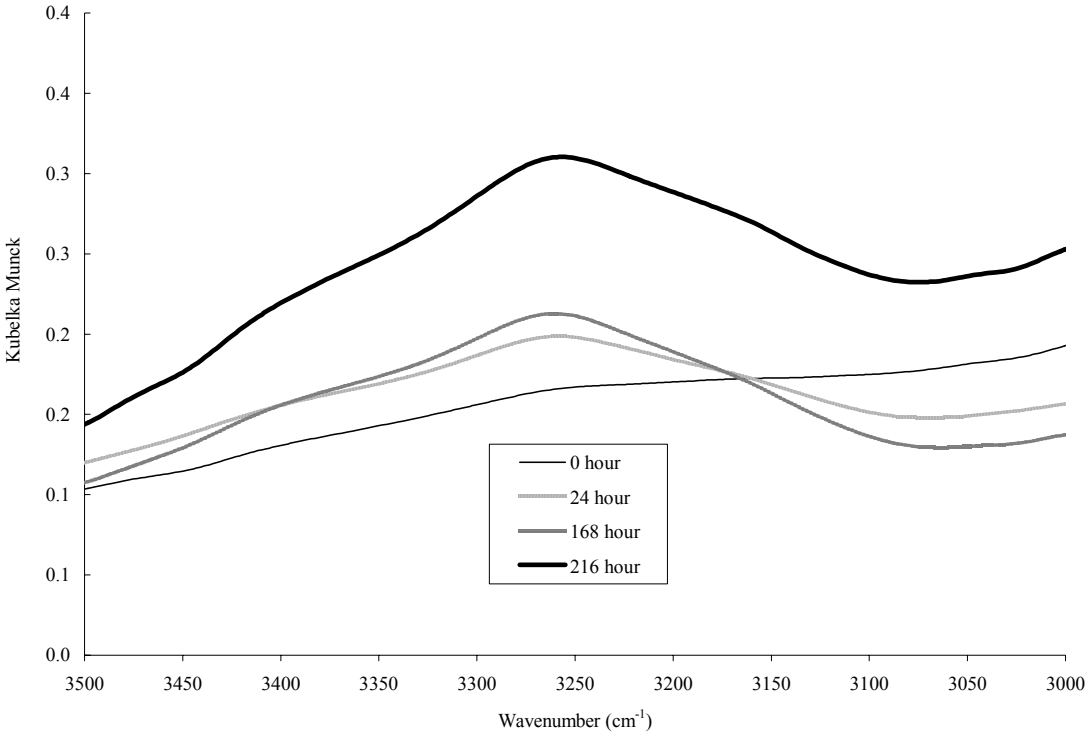

Figure 3.6. FTIR spectra for float glass treated with Laemmli buffer + PEG as a function of treatment time.

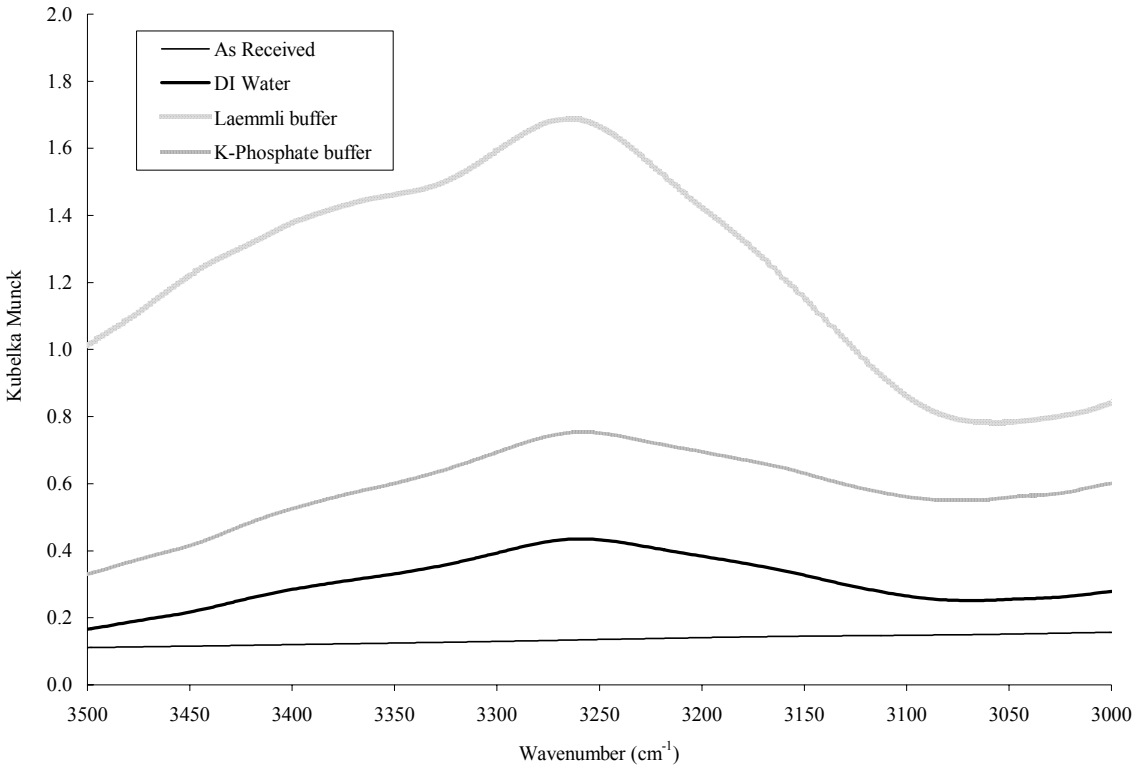

Figure 3.7. FTIR spectra for as-received float glass and samples immersed in DI water, Laemmli buffer and K-phosphate buffer for 216 hours.

3.2.3. EIS

An impedance summary is shown in Figure 3.8, with the |Z| values taken at a frequency of 1Hz. The variation from sample to sample and treatment to treatment can be explained by looking at the noise observed in the low frequency region of Figure 3.3 and will be discussed later.

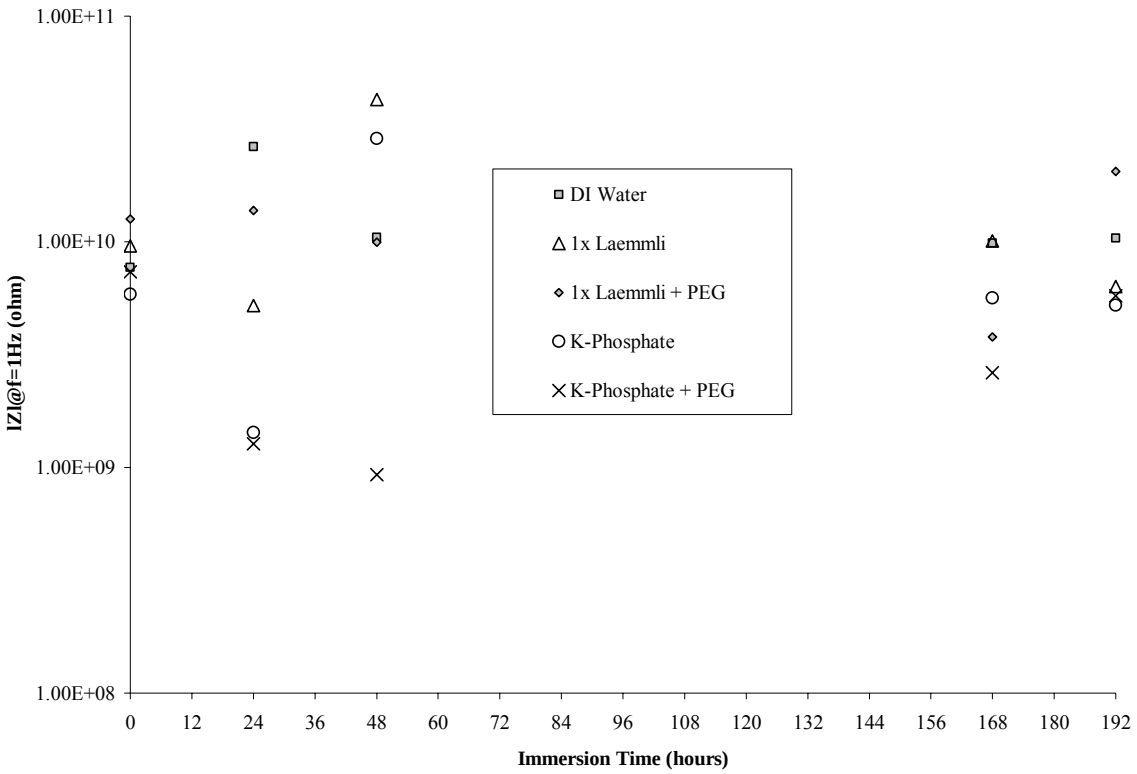

Figure 3.8. Average impedance at 1Hz for float glass as a function of treatment time.

3.2.4. Electrophoresis

Figure 3.9 - Figure 3.11 show the results of three electrophoresis experiments with the treated float glass substrates. The I/A values for the glass seen in Figure 3.9, Figure 3.10, and Figure 3.11 were calculated to be 1.64, 7.05 and 60.57mA/mm^2, respectively. It is important to note that each sample clearly showed electroosmotic and electrophoretic flow patterns.

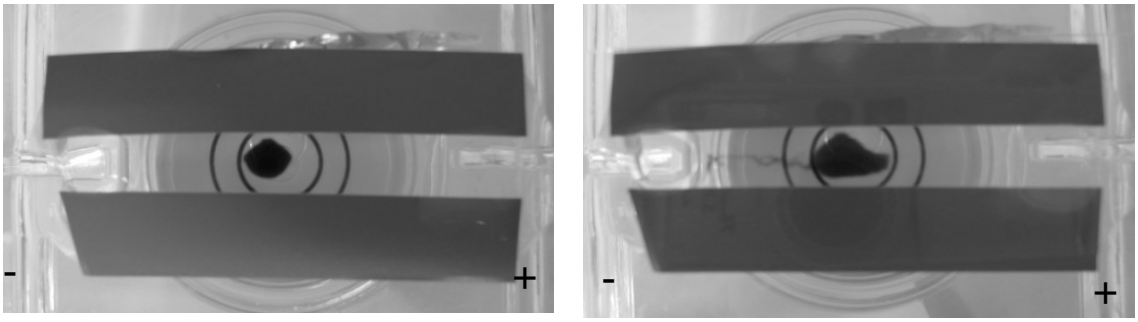

Figure 3.9. Float glass treated for 192 hours in 1x Laemmli buffer + PEG at t=0 (left) and t=21 minutes (right) with a 200V applied potential and a 1μL drop of bpb. Current per cross sectional area was 1.64 mA/mm^2.

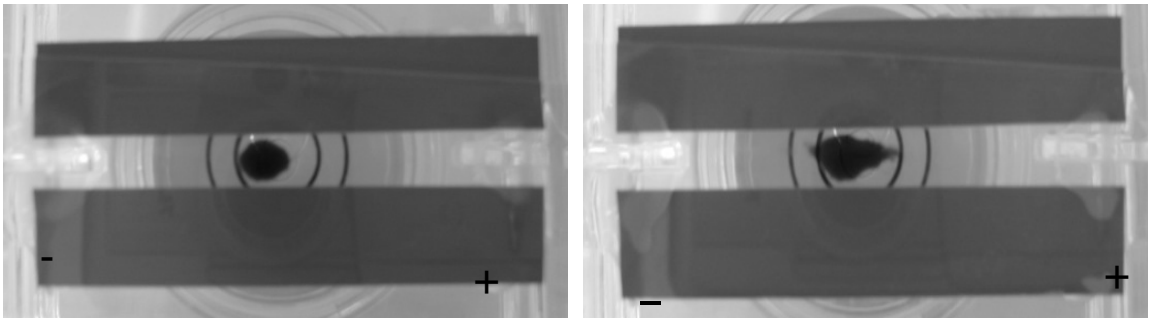

Figure 3.10. Float glass treated for 192 hours in 1x Laemmli buffer + PEG at t=0 (left) and t=22 minutes (right) with a 200V applied potential and a 1μL drop of bpb. Current per cross sectional area was 7.05 mA/mm^2.

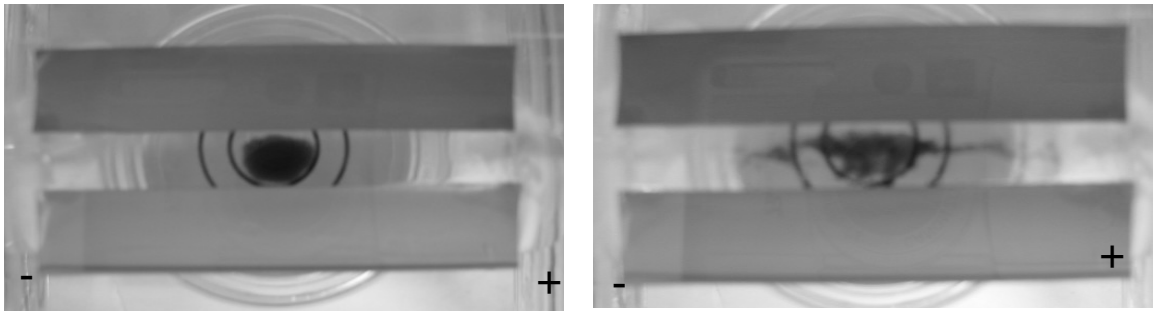

Figure 3.11. Float glass treated for 192 hours in K-Phosphate buffer at t=0 (left) and t=6 minutes (right) with a 200V potential applied and a 1μL drop of bpb. Current per cross sectional area was 60.57 mA/mm^2.

3.3. 33% Sodium

3.3.1. Contact Angle Analysis

A summary of contact angle measurements as a function of treatment time can be seen in Table V. The plasma treated contact angles are similar to the other glass compositions, with the exception being float glass. The 33% sodium is a very non-durable glass for which surface cracks developed when the sample was removed from the treatment solution and allowed to dry in the ambient environment. The surface cracking occurred because the glass surface contained a high amount of water when it was removed from solution and the air drying process in relatively low humidity allowed for rapid evaporation.

Table V. Contact Angle Measurements for 33% Sodium Glass

Treatment Solution	As-Rec'd	After Plasma	24 hour	48 hour	60 hour
DI Water	18.3º ± 2.9	5.9º ± 1.8	13.5º ± 3.2	10.5º ± 3.2	8.5º ± 2.7
1x Laemmli Buffer		7.1º ± 1.7	13.8º ± 3.7	13.0º ± 4.6	11.2º ± 3.9
1x Laemmli Buffer plus PEG		6.5º ± 2.0	11.0º ± 2.3	12.8º ± 4.2	13.1º ± 3.9
		After Plasma	24 hour	48 hour	96 hour
K-Phosphate Buffer		5.1º ± 1.4	12.1º ± 2.4	13.5º ± 4.2	10.9º ± 2.0
K-Phosphate Buffer plus PEG		5.0º ± 1.3	10.4º ± 2.6	10.9º ± 2.3	11.2º ± 1.9

3.3.2. FTIR

Figure 3.12 and Figure 3.13 show the spectra for a sample treated in Laemmli buffer + PEG and the final spectra collected for samples treated in DI water, Laemmli and K-Phosphate buffers, respectively. Each spectra contained in the two figures have been baseline corrected to account for variations in the intensity of each signal and smoothed to remove the small amount of noise. The surface cracking affected the original data because the signal intensity varied more in this glass than any other. Since

the surface was not uniform, the IR light may have reflected at other angles, thus making the intensity vary. Although the surface was not uniform, the important features within the hydroxyl region can be seen easily.

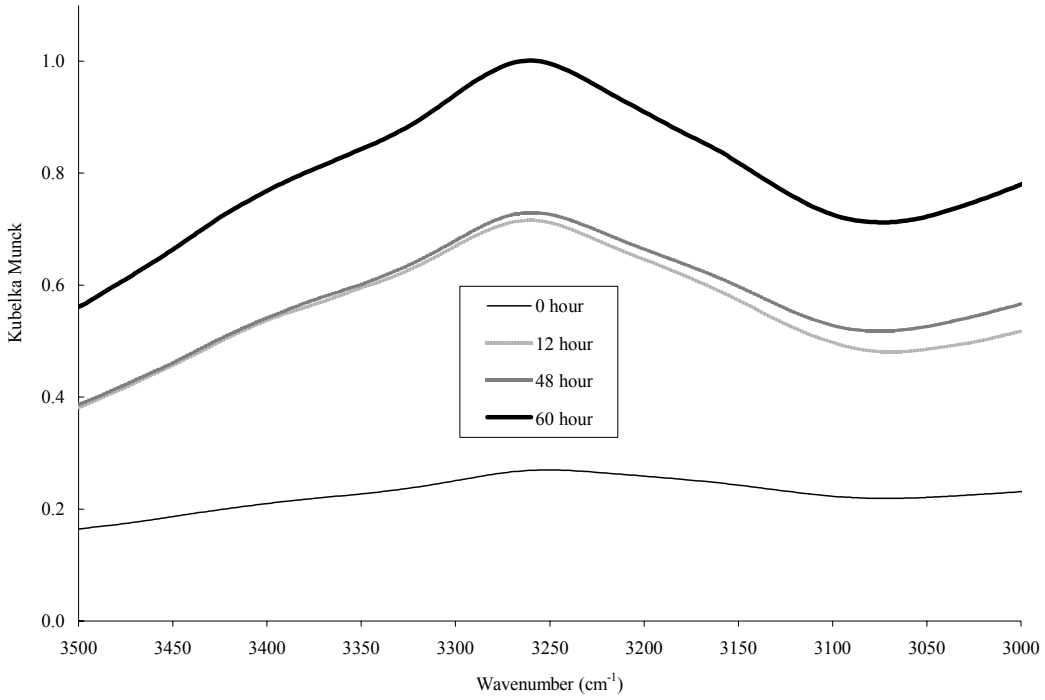

Figure 3.12. FTIR spectra for 33% sodium silicate glass immersed in Laemmli buffer + PEG as a function of treatment time.

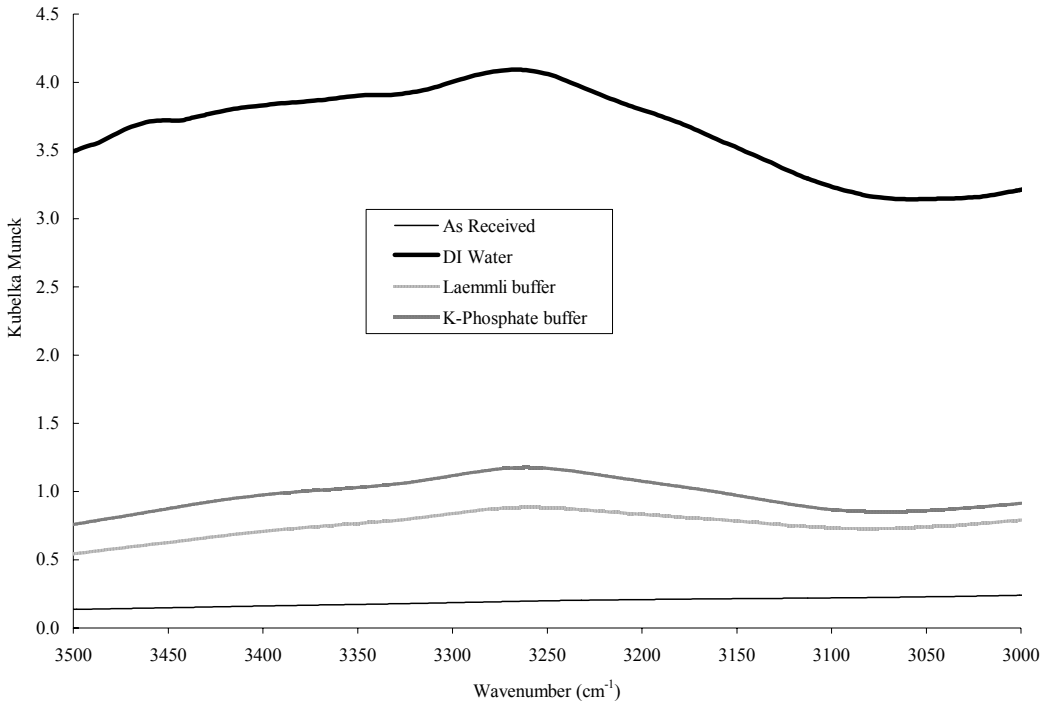

Figure 3.13. FTIR spectra for as-received 33% sodium silicate glass and samples immersed in DI water and Laemmli buffer for 60 hours and K-phosphate buffer for 96 hours.

3.3.3. EIS

Bode plots for a 33% sodium glass treated in K-Phosphate buffer are shown in Figure 3.14. This composition was the only one that resulted in a low amount of noise in the low frequency region. There was very little noise, even in the time zero measurement. When the buffer was placed in the channel, the impedance spectrum looks qualitatively similar to the K-Phosphate buffer impedance presented in Figure 2.4, but the impedance is two orders of magnitude higher when the glass was tested. In general, the 33% sodium glass exhibited less noise in the lower frequency range than the other glasses. This was the least durable of the compositions tested and is therefore extremely reactive to water species.

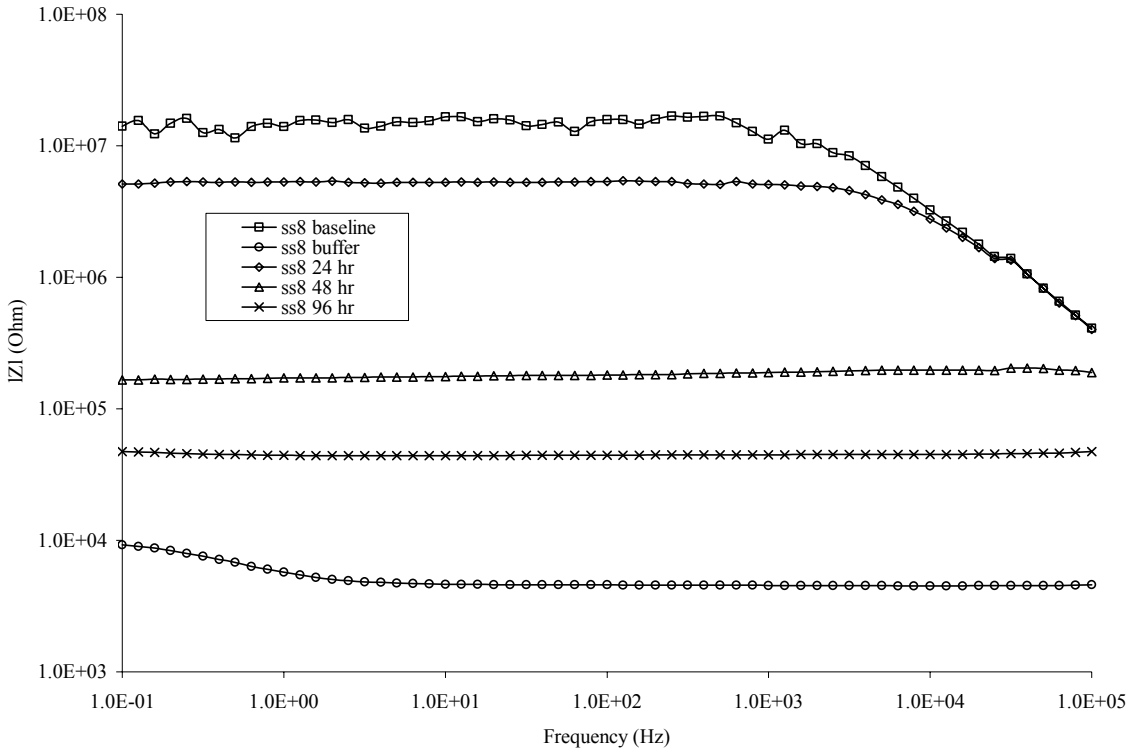

Figure 3.14. Bode plots for 33% sodium glass treated with K-Phosphate buffer at various treatment times.

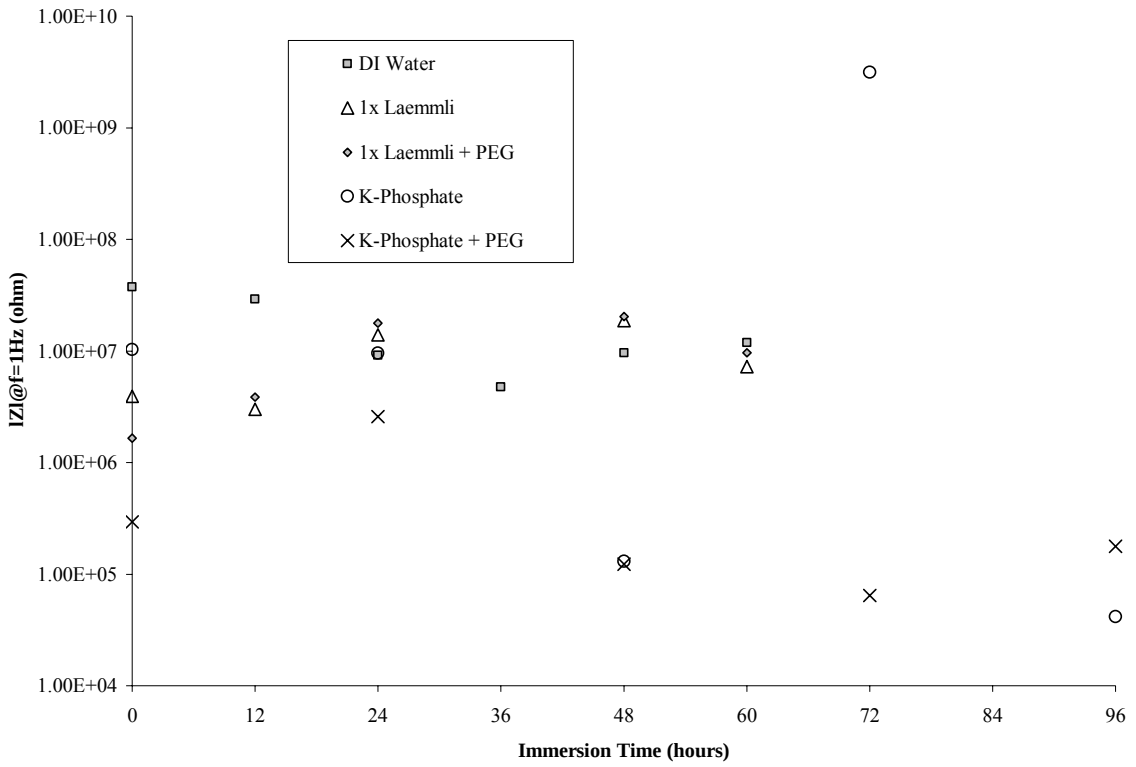

Figure 3.15. Average impedance at 1Hz for 33% sodium silicate glass as a function of treatment time.

3.3.4. Electrophoresis

The 33% sodium glass showed terrific results in the electrophoresis experiments, however, the surface cracking may have played a significant role in the observed success. The calculated I/A values for Figure 3.16, Figure 3.17, and Figure 3.18 were 49.65, 32.43, and 20.88mA/mm^2, respectively. Although the glass did support electrical current flow, it is thought that the dye moving through the cracks significantly aided the migration in this glass. The surface cracking observed in this glass indicates that it is not suitable for microfluidic applications because the amount and size of the surface cracks could vary from sample to sample, resulting in surface inconsistencies.

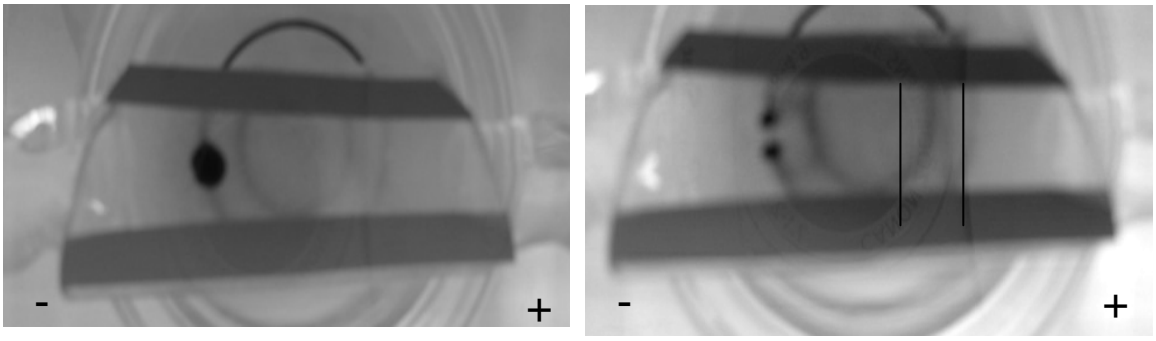

Figure 3.16. 33% sodium silicate glass treated for 60 hours in 1x Laemmli buffer at t=0 (left) and t=3 minutes (right) with a 200V applied potential and a 0.5μL drop of bpb. The lines in the right photograph show the start line (left) and ending line (right). Current per cross sectional area was 49.65 mA/mm^2.

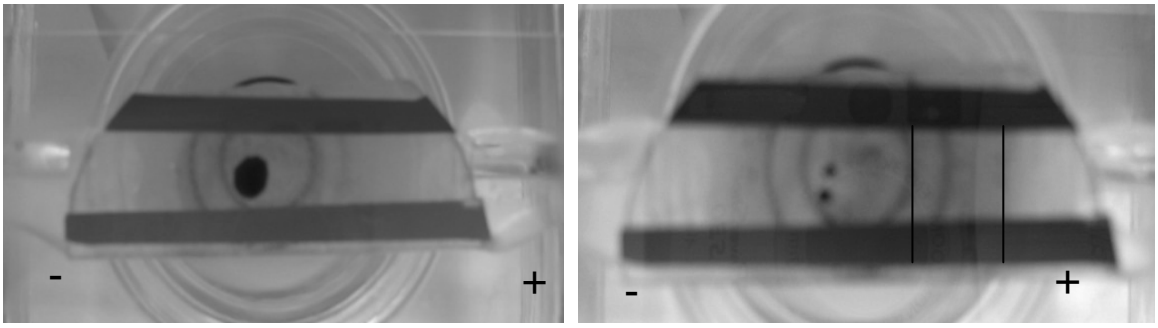

Figure 3.17. 33% sodium silicate glass treated for 60 hours in 1x Laemmli buffer + PEG at t=0 (left) and t=3 minutes (right) with a 200V potential applied and a 0.5L drop of bpb. Current per cross sectional area was 32.43 mA/mm^2. The lines in the right photograph show the starting and ending point for the tracer dye.

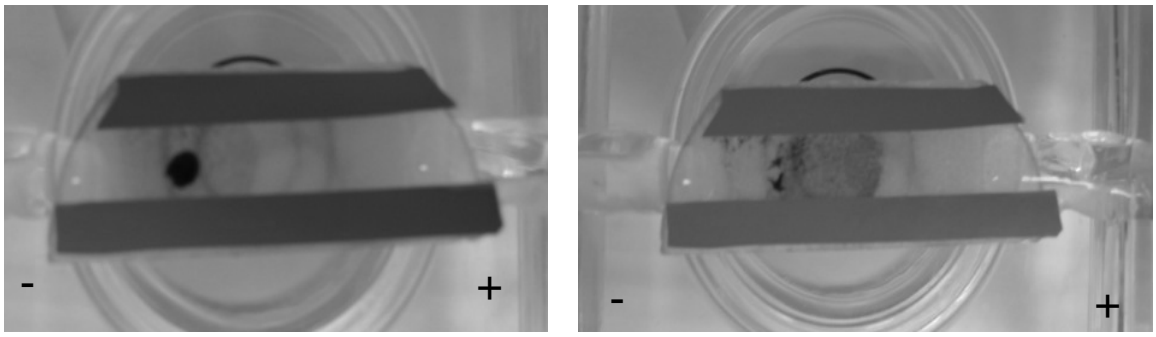

Figure 3.18. 33% sodium silicate glass treated for 60 hours in 1x Laemmli buffer + PEG at t=0 (left) and t=3 minutes (right) with a 200V potential applied and a 0.5μL drop of bpb. Current per cross sectional area was 20.88 mA/mm^2.

3.4. 24% Sodium

3.4.1. Contact Angle Analysis

Table VI shows the contact angle of the 24% sodium as a function of immersion time for each solution. The as-received and plasma treated contact angles are within one standard deviation of the angles measured for the 33% sodium composition. However, the final contact angles for the two compositions varied significantly.

Table VI. Contact Angle Measurements for 24% Sodium Glass

Treatment Solution	As-Rec'd	After Plasma	24 hour	48 hour	60 hour
DI Water	16.5º ± 2.4	9.5º ± 2.5	33.7º ± 5.7	35.4º ± 5.2	30.4º ± 8.3
1x Laemmli Buffer		8.2º ± 1.7	19.9º ± 2.3	19.5º ± 3.5	17.3º ± 3.5
1x Laemmli Buffer plus PEG		8.0º ± 1.7	16.4º ± 2.9	16.6º ± 2.8	16.3º ± 2.7
K-Phosphate Buffer		5.7º ± 1.4	21.9º ± 3.9	25.7º ± 4.0	25.9º ± 2.7
K-Phosphate Buffer plus PEG		5.2º ± 1.6	19.2º ± 2.7	26.3º ± 3.8	26.6º ± 3.6

3.4.2. FTIR

The IR spectra for the 24% sodium glass clearly show a change in the surface as treatment time progresses. Figure 3.19 shows the spectra as a function of time for glass immersed in DI water for up to 60 hours. The time zero spectra shows little activity within the range of interest and as time progresses peaks form at 3260 and 3410cm^{-1}. Figure 3.20 shows the as-received glass and compares it to glass treated in DI water, Laemmli buffer, and K-Phosphate buffer for 60 hours. Each treatment resulted in the formation of peaks in the hydroxyl region. Each of the two figures have been baseline corrected to account for variations in the intensity of each signal and smoothed to remove the small noise.

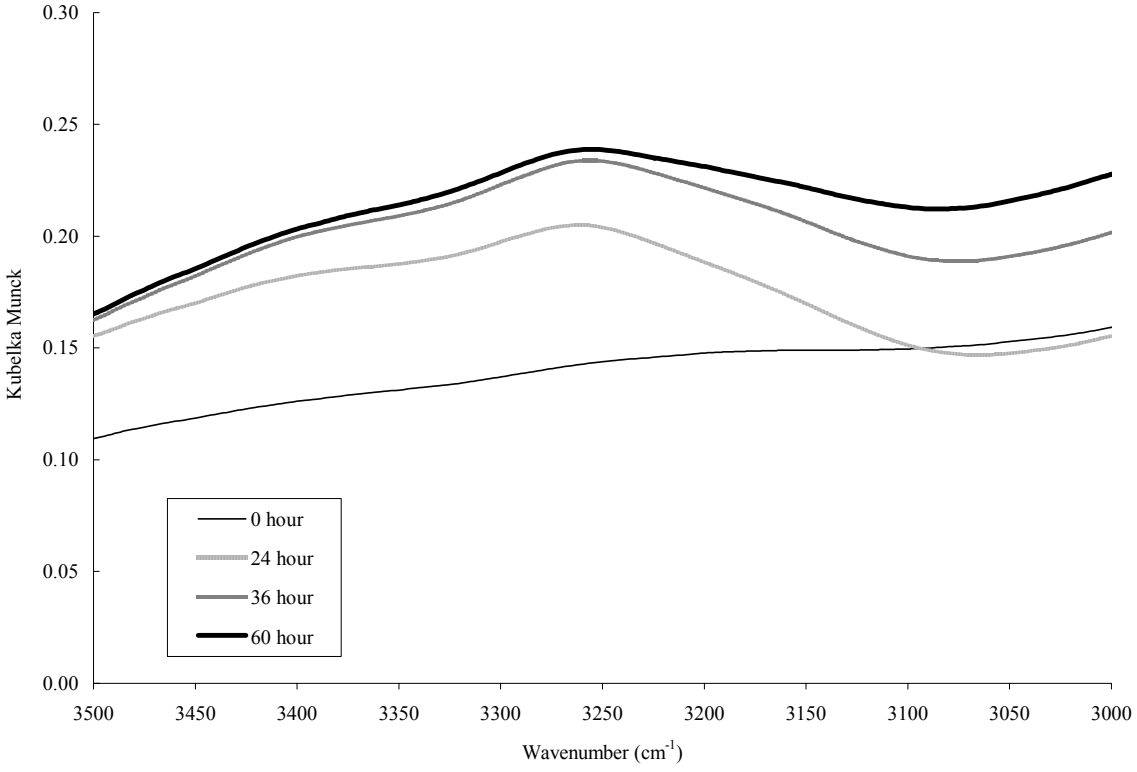

Figure 3.19. FTIR spectra for 24% sodium silicate glass immersed in DI water as a function of treatment time.

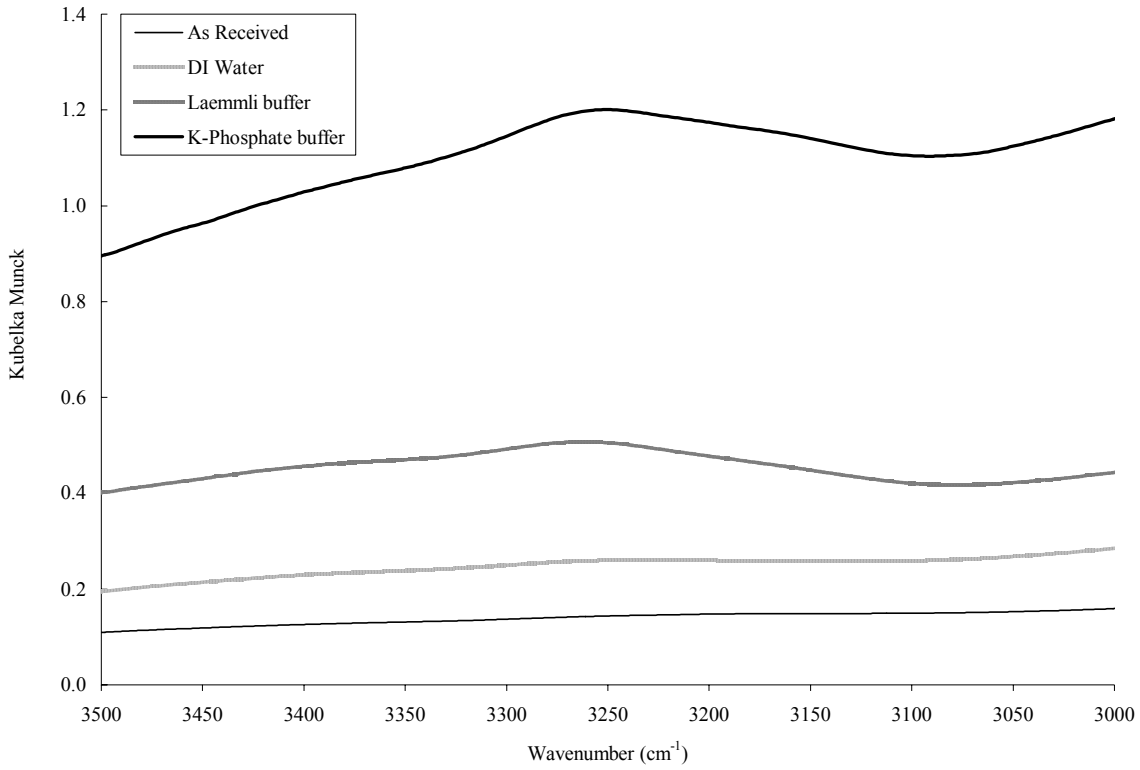

Figure 3.20. FTIR spectra for as-received 24% sodium silicate glass and samples immersed in DI water, Laemmli buffer and K-phosphate buffer for 60 hours.

3.4.3. EIS

Figure 3.21 shows the impedance at 1Hz for the treated glass. As was the case with the other compositions, the noise in the low frequency region influenced the data.

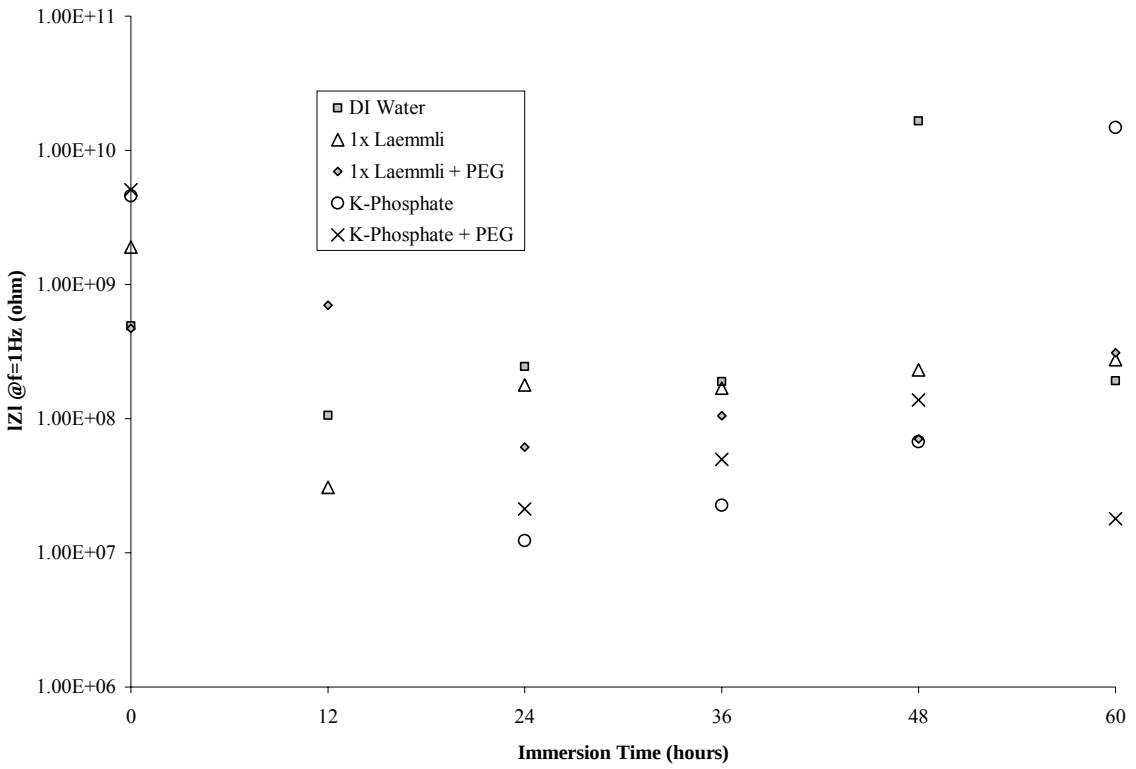

Figure 3.21. Average impedance at 1Hz for 24% sodium silicate glass as a function of treatment time.

3.4.4. Electrophoresis

Electrophoresis photographs are included for 60, 108 and 180 hour treatments in K-Phosphate buffer. The I/A values for the three treatment times were 0.000, 0.044 and 0.229mA/mm^2, respectively. These values were much lower than the values calculated for the other compositions. Originally, the glass was treated for 60 hours, equivalent to the treatment time for the 33% sodium glass. Initially, no migration was observed and the glass was treated for additional time since decreasing sodium content will increase durability. They were re-tested after 108 and 180 hours and still no migration was observed. Also, the cracks that developed in the 33% sodium glass after 60 hours did not form in the 24% glass even after 180 hours of treatment. Although the sodium content was decreased, and thus durability improved, this glass should have been less durable than the SLS and float glasses. Since the float glass showed migration, this glass was expected to be able to support migration based on the relative durability's. The higher contact angles in this composition indicate that there is more water species present on the

surface, since the addition of hydroxyl groups will lower the surface energy and increase contact angle and therefore does not provide an explanation for the lack of migration.

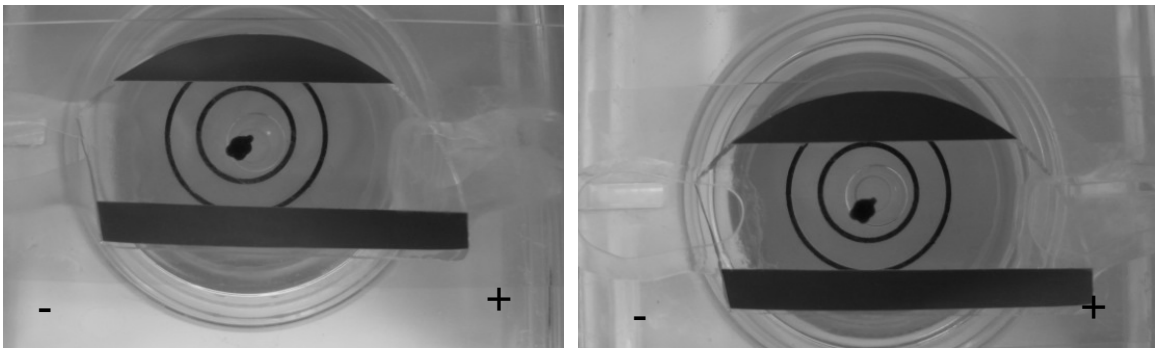

Figure 3.22. 24% sodium glass treated for 60 hours in K-Phosphate buffer at t=0 (left) and t=20 minutes (right) with a 200V applied potential and a 0.1μL drop of bpb. Current per cross sectional area was 0.00 mA/mm^2.

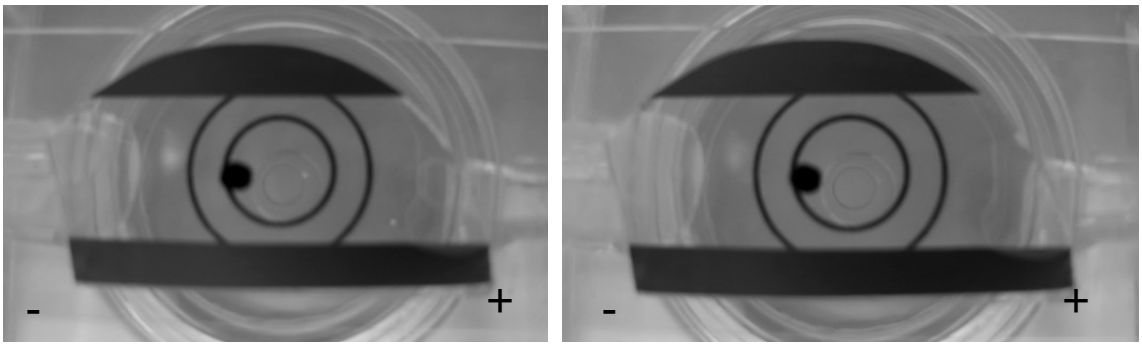

Figure 3.23. 24% sodium glass treated for 108 hours in K-Phosphate buffer at t=0 (left) and t=6 minutes (right) with a 200V applied potential and a 0.1μL drop of bpb. Current per cross sectional area was 0.044 mA/mm^2.

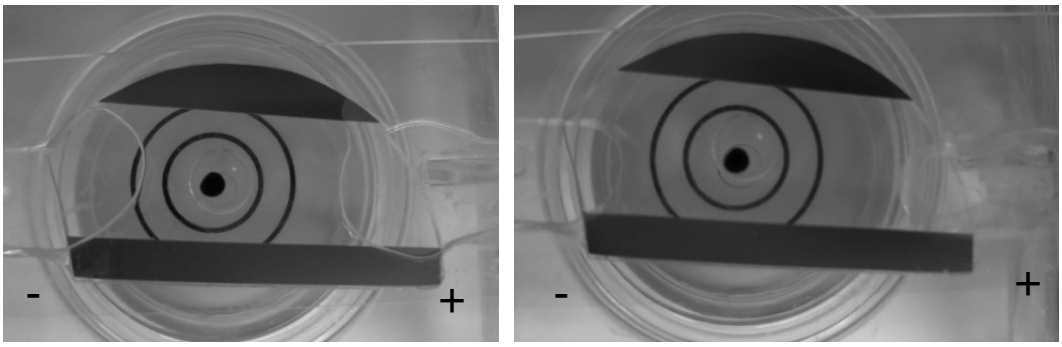

Figure 3.24. 24% sodium glass treated for 180 hours in K-Phosphate buffer at t=0 (left) and t=20 minutes (right) with a 200V applied potential and a 0.1μL drop of bpb. Current per cross sectional area was 0.229 mA/mm^2.

3.5. Phosphate Glass

3.5.1. Contact Angle Analysis

Table VII shows the contact angle for phosphate glass as a function of immersion time. The phosphate glass had low as-received contact angles, and the plasma treated angles were similar to the other compositions.

Table VII. Contact Angle Measurements for Phosphate Glass

Treatment Solution	As-Rec'd	After Plasma	24 hour	36 hour	60 hour
DI Water	14.6º ± 3.2	4.4º ± 1.5	26.3º ± 4.4	30.4º ± 4.6	31.2º ± 5.3
1x Laemmli Buffer	15.9º ± 3.1	3.0º ± 1.6	16.3º ± 3.7	15.1º ± 4.9	14.8º ± 4.5
1x Laemmli Buffer plus PEG	15.5º ± 3.5	3.9º ± 1.3	10.5º ± 2.2	11.1º ± 1.9	11.0º ± 2.2
K-Phosphate Buffer	15.6º ± 3.1	4.0º ± 1.5	11.1º ± 1.9	11.4º ± 1.8	10.3º ± 3.1
K-Phosphate Buffer plus PEG	17.3º ± 3.4	4.4º ± 1.3	10.5 ± 2.1	10.9º ± 2.1	11.0º ± 2.5

3.5.2. FTIR

The IR spectra as a function of treatment time show that the as-received glass did not contain a measurable amount of hydroxyl groups or water on the surface. As seen in the other compositions as treatment time increased, peaks began to form in the hydroxyl region indicting the formation of water containing species on the surface. Also seen in other glasses, Figure 3.26 shows the effect of DI water, Laemmli buffer and K-Phosphate buffer treatment with respect to the as-received surface. Each treatment allowed for the formation of water species at the surface. The phosphate electrophoresis photographs seen in Figure 3.29-Figure 3.31 correspond to the spectra seen in Figure 3.25.

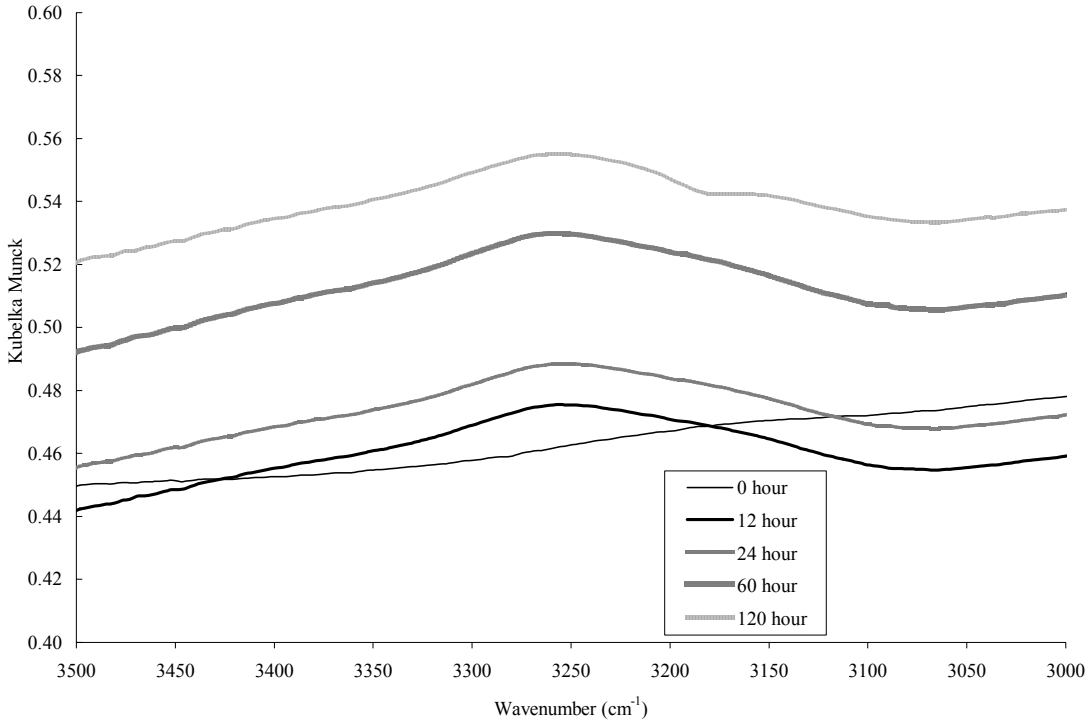

Figure 3.25. FTIR spectra of phosphate glass immersed in Laemmli buffer at various time intervals.

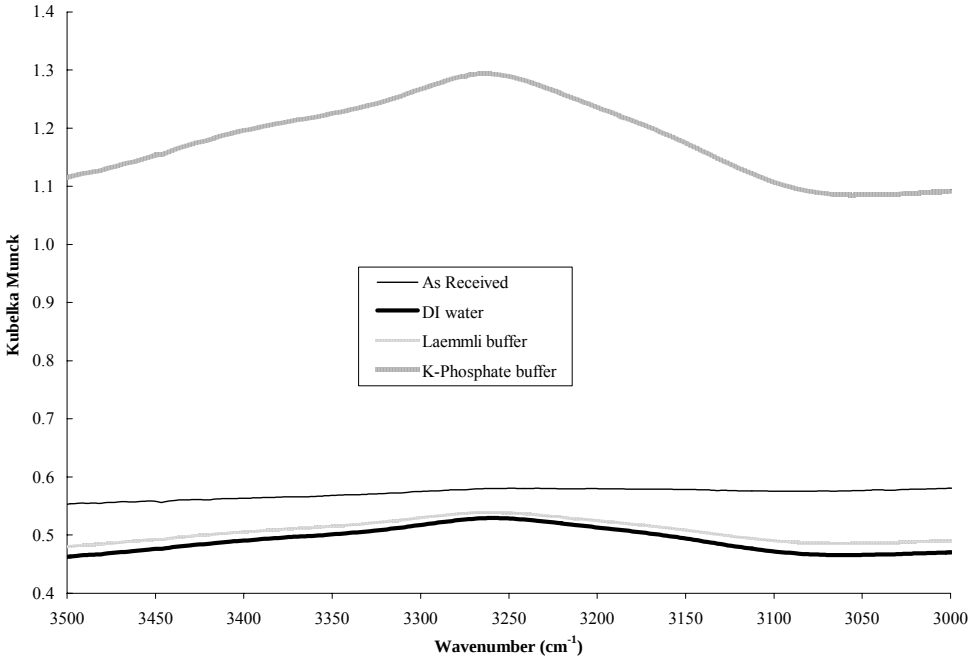

Figure 3.26. FTIR spectra for as-received phosphate glass and samples immersed in DI water, Laemmli buffer and K-phosphate buffer for 190 hours.

3.5.3. EIS

Impedance was measured for the phosphate glass at two distances between the agarose gels on the surface. The gels were tested with separation distances of 1cm and 2cm. For the technique that was used to apply the gel, 1cm was the closest that the gels could be placed reproducibly without connecting them. This was done to see if impedance was dependent on the distance between the gels. In both cases, noise was still present in the low frequency range. Figure 3.27 shows the impedance summary at 1Hz when the gel separation distance was 2cm and Figure 3.28 is the impedance data for gel separation distances of 1cm.

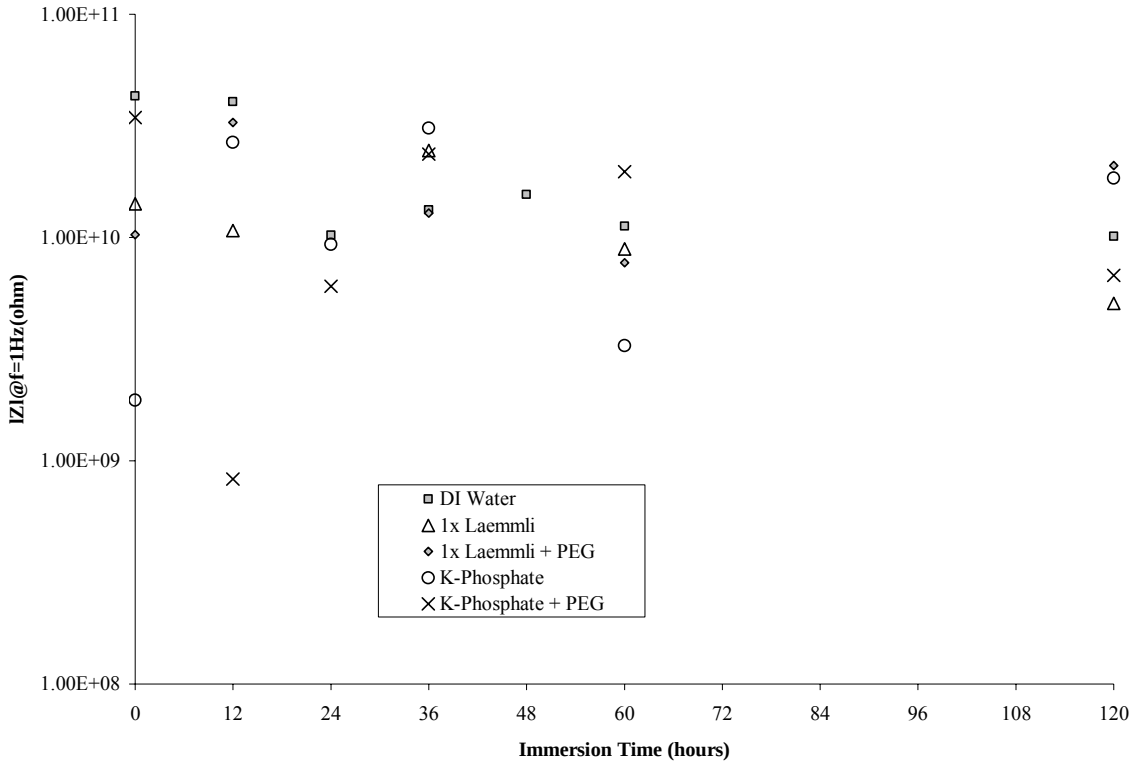

Figure 3.27. Average impedance at 1Hz for phosphate glass when gel was placed ~2cm apart as a function of treatment time.

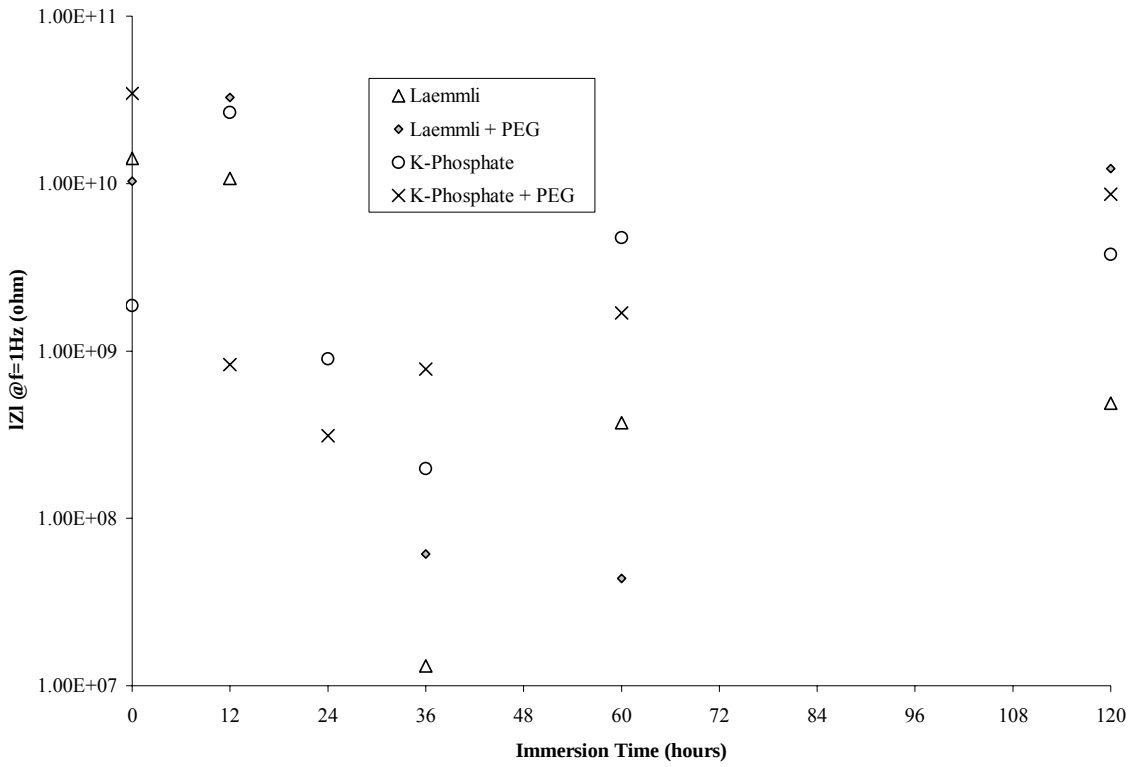

Figure 3.28. Average impedance at 1Hz for phosphate glass when gel was placed ~1cm apart as a function of treatment time.

3.5.4. Electrophoresis

The treated phosphate glass yielded promising electrophoresis results. Fluid migration occurred in more of the samples than any of the previous compositions. The observed migration was more pronounced using the phosphate, seen in Figure 3.29-Figure 3.33, than the silicate glasses. Also, a higher percentage of the samples were able to support current flow (measured by the voltammeter), about 90% compared to the silicate glass compositions in which about 80% were able to support current flow.

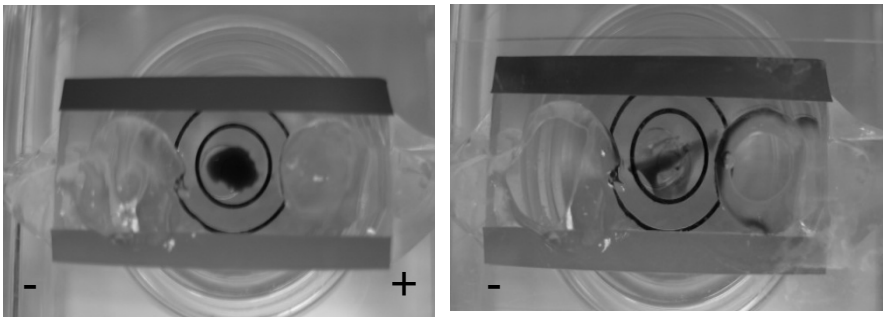

Figure 3.29. Phosphate glass treated for 60 hours in 1x Laemmli buffer at t=0 (left) and t=10 minutes (right) with a 200V applied potential and a 0.1μL drop of bpb. Agarose gel separation ~1cm. Current per cross sectional area was 6.11 mA/mm^2

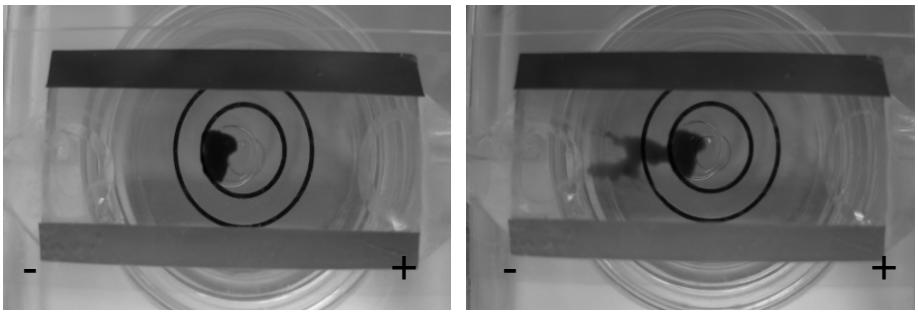

Figure 3.30. Phosphate glass treated for 60 hours in 1x Laemmli buffer at t=0 (left) and t=10 minutes (right) with a 200V applied potential and a 0.1μL drop of bpb. Agarose gel separation ~2cm. Current per cross sectional area was 0.337 mA/mm^2

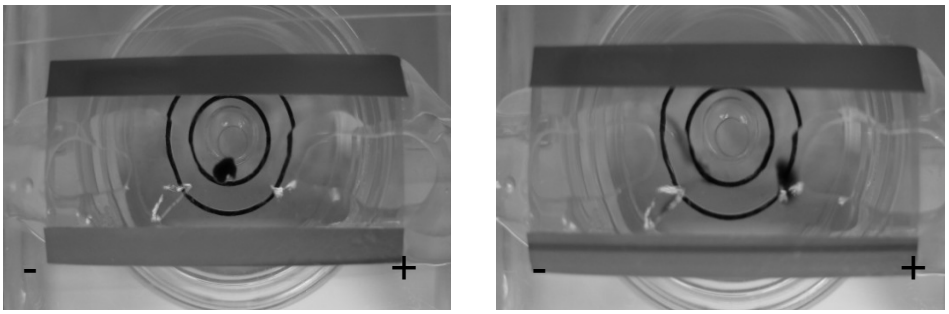

Figure 3.31. Phosphate glass treated for 120 hours in 1x Laemmli buffer at t=0 (left) and t=10 minutes (right) with a 200V applied potential and a 0.1μL drop of bpb. Agarose gel separation ~1cm. Current per cross sectional area was 8.15 mA/mm^2

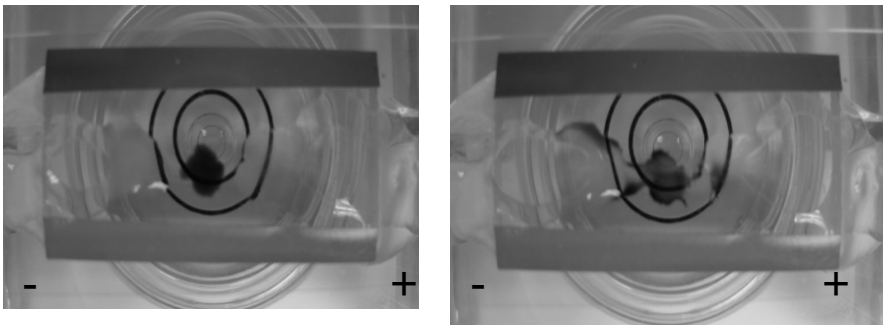

Figure 3.32. Phosphate glass treated for 120 hours in 1x Laemmli buffer at t=0 (left) and t=15 minutes (right) with a 200V applied potential and a 0.1μL drop of bpb + hemoglobin. Agarose gel separation ~1cm. Current per cross sectional area was 4.57 mA/mm^2

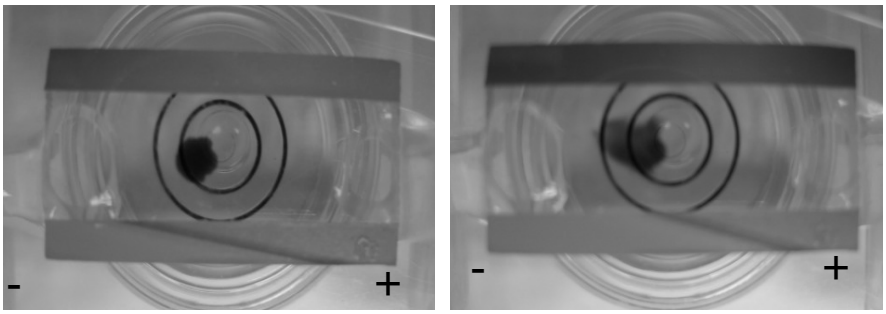

Figure 3.33. Phosphate glass treated for 120 hours in 1x Laemmli buffer + PEG at t=0 (left) and t=10 minutes (left) with a 200V applied potential and a 0.1μL drop of bpb + hemoglobin. Agarose gel separation ~2cm. Current per cross sectional area was 0.17 mA/mm^2

Similar to the impedance measurements, the electrophoresis experiment was tested with two gel separation distances, 2cm and 1cm which can be clearly seen in the included photographs. When the separation distance of the agarose gel was decreased, the effective length of the channel was decreased, which resulted in lower electrical loss through the channel. The current per cross sectional area (I/A) values for the smaller separation distances were greater than the values calculated for the larger separation distances. Table VIII shows how I/A changes with exposure time and separation distance. Although the results were somewhat expected, it's still worthwhile to note the trend. It is also worth noting that the Laemmli buffer provided better fluid migration after 120 hours of treatment than the K-Phosphate buffer, even though the I/A is higher for the K-Phosphate sample.

Table VIII. Comparison of calculated I/A values for phosphate glass treated in Laemmli and K-Phosphate buffer as a function of treatment time.

		I/A (mA/mm^2) for	
Treatment	Time (hours)	1cm	2cm
Laemmli buffer	60	6.11	0.34
	120	8.15	3.21
K-Phosphate buffer	60	3.75	0.14
	120	19.75	5.40

4. Discussion

Overview: The relationship between the results from the experimental methods is discussed. Initially, the contact angle decreases because hydroxyl groups are added to the surface during the water plasma treatment. The hydroxyl groups on the surface interact with the water drop and cause it to spread. During the progression of the treatment, a hydrated layer consisting of hydroxyl groups and water is formed in the near sub-surface region. As a direct result, the intensity of the hydroxyl region in the IR spectra is expected to increase and the channel impedance should decrease. The final result is a surface that can support current flow and fluid migration. Each of these concepts are discussed separately.

Contact Angle and Infrared Spectroscopy: The low contact angle, seen after plasma treatment of the glasses, can be attributed to the hydroxyl groups that are added to the surface region during the seven minute treatment. The contact angle with a liquid that is similar to the surface (water) is low because the liquid spreads over the surface. The hydroxyl groups may not have been seen in the IR spectra because of the lack of immediate surface sensitivity of the grazing angle chosen (80º). As aqueous treatment in UV radiation proceeded, the contact angle increased which would indicate that the surface was becoming less water-like and hydroxyl group density of the immediate surface was decreasing. This may be due to the adsorption of contaminants to the surface from the environment during the times it was not in solution. The surface hydroxyl groups play an important role in the surface properties since they can act as an effective adsorption or reactive site.[50] Environmental contaminants include any impurity in the laboratory atmosphere, especially organic species that can react with the hydroxyl group and bond with the oxygen atom. Again, the adsorption of contaminants was not observed in the IR spectra; however, the immediate surface sensitivity may not have been high enough using an 80º from the normal incident angle. If a contamination layer was formed on the surface, the contact angle would not be affected by the water present in the hydrated layer that is formed during the UV treatments because the water drop used in

contact angle measurements interacts with the immediate surface only.[51] If the surface remained hydroxylated, the wetting behavior of the glass would persist throughout the aqueous treatments and the contact angle would remain low (as in the case of the plasma treated surface).

The IR spectra of all of the glass compositions show a marked increase in the hydroxyl region intensity with increasing treatment time. This confirms the idea that the surface region is being altered and water is being introduced into the system. The water can take the form of molecular water that attaches to the surface or diffuses into the structure, or hydroxyl groups that are present as silanol species. Each water species has a characteristic vibration frequency that can be measured in the IR region. The most significant changes for each composition were seen at 3260cm^{-1}, which is a vibrational frequency of molecular water.

Impedance Spectroscopy: Unfortunately, the noise in the lower third of the frequency range made it difficult to draw definitive conclusions from the impedance data. The noise associated with the low frequency impedance can be attributed to the resistive nature of the glass. The figures showing the impedance as a function of immersion time at 1Hz have substantial variation within the data, approximately two orders of magnitude. In an attempt to quantify the variation, a best fit line was adapted to the data set. Different regression techniques (power, linear, exponential, logarithmic and polynomial) were used to attempt to quantify the variation of the data. A small r-squared value was expected, since the noisy data set was going to be approximated by a single line. The best fit resulted in an r-squared value of 0.05. However, none of the computer regression models fit the data in a way that seemed to take all of the points into account. When the separation distance for the impedance measurement was reduced on the phosphate glass, the noise was still a factor in the low frequency realm. Again, the variation in the data was fit using regression techniques but r-squared values in the 0.009 region resulted.

Electrophoresis: Interestingly, the electrophoresis experiments resulted in various migration patterns. Ideally, the glass surfaces treated in the same solution should have similar properties and therefore result in similar flow patterns. Some samples within the same composition and treatment exhibited only EOF, while others showed electrophoretic flow and still others displayed both. It was thought that one property that

should affect the flow pattern is the current per cross sectional area. An attempt was made to correlate the flow patterns to the calculated current per cross sectional area in order to predict the expected flow based on current, but no direct correlations emerged. Even within each composition, there is no trend to the calculated current per cross sectional area and the flow that was observed. The variability of the agarose connection to gel rig may have also affected the electrophoresis results. The agarose gel was applied to each sample using a pipette, which did not dispense the same amount of gel each time and was subject to variations in application.

Analysis of the contact angles indicated that the measured angles may be linked to successful fluid migration. All of the treatments that performed well in electrophoresis had average contact angles in the teens. This is not to say that a sample with an average contact angle in the teens guaranteed successful migration, but rather, that the samples with average contact angles in the teens had a better chance of being successful, or showing electrokinetic migration. Treatments that resulted in contact angles in the twenties and low thirties did not provide migration. The surfaces with higher contact angles may have had a more dehydroxylated surface with contaminants present which could be detrimental to the electrokinetic flow.

In the end, the phosphate glass showed the most consistency during electrophoresis. More specifically, the phosphate glass treated with Laemmli buffer yielded the most promising results. Since phosphate glasses are generally not very durable, the formation of hydroxyl groups is favored. The deprotonation of the hydroxyl groups may play an important role in forming the surface layer. Surface charge plays an important role in electrokinetic migration so the surface charge could be one explanation of the success that was seen with the phosphate glass that was not seen with the silicate glasses. As discussed previously, the presence of negative surface charge is the driving force behind electroosmotic flow.

One explanation for the presence of surface charge on the glass is the point-of-zero charge (pzc) of the major glass components. The pzc is the point at which the species is charge neutral. At pH values below the pzc, equation (3) dominates and the result is a positive charge. At pH values above the pzc, equation (4) controls and results in a negative charge.

$$M\text{-}OH + H^+ \rightarrow M\text{-}OH_2^+ \quad (3)$$

$$M\text{-}OH + OH^- \rightarrow M\text{-}O^- + H_2O \quad (4)$$

The pzc for SiO_2 is between 2 and 3.7.[52] The treatment solutions tested in the current study were pH 5.8, ~7 and 8.0. This would suggest that the silicate glass surfaces that were tested had at least some negative character which contributed to the electroosmotic flow that was seen in the photographs. A pzc for P_2O_5 was not found in literature probably because of the tendency for the rapid formation of phosphoric acid when it is added to water. A pzc was also not available for aluminophosphate glass, which is the type used in the current investigation.

5. Conclusions

A variety of glass compositions were exposed to aqueous solutions and the surface reactions were monitored. IR spectroscopy and contact angle analysis proved to be useful techniques for characterizing the glass surfaces during treatment. Each provided a quick analysis of the glass, while not significantly disrupting the treatments.

It was found, through the contact angle measurements, that the glass surface initially had a low contact angle after plasma treatment due to the presence of hydroxyl groups that were added during the plasma treatments. As the aqueous solution UV exposure treatments progressed, the contact angle increased for all compositions, indicating the possible presence of surface contaminants that were not seen using IR spectroscopy. Samples that consistently maintained a low contact angle, < 20 degrees, showed the best electrokinetic flow behavior. The IR spectroscopy measurements support the hydrated layer formation claim. Specifically, the region between 3500-3000cm^{-1} showed increased activity as treatment time increased. This confirmed that water was being incorporated into the surface and sub-surface structure during the aqueous treatments.

The impedance measurements did not yield the results originally hypothesized. Instead of observing decreasing channel impedance as a function of treatment time, noise from the glass in the low frequency range distorted the data. While testing the phosphate glass, the gel separation distance was reduced to 1cm to test the effect of a shorter effective glass surface. The variations were still observed in the low frequency region of the spectra. The technique for applying the gel to the glass made it difficult to place the gel closer than 1cm reproducibly, but there does not seem to be a correlation between impedance and separation distance. Only the sodium silicate samples showed reasonable impedance data with low noise in the low frequency region. The 33% sodium glass was the least durable of all the compositions and the amount of water that was present within the network probably influenced the impedance measurements.

The phosphate glass treated provided the best electrophoresis results. The reactions that formed the hydrated layer were no doubt affected by the network forming atoms in each of the glasses. The solution pH also influenced the electrophoresis results, especially in the phosphate glass. Fluid migration was seen in the phosphate glasses that were treated in pH 8.0 Laemmli buffer and was not seen in treatments with pH 5.8 K-phosphate buffer. The treatment pH did not affect fluid migration on the silicate glasses, migration occurred on float glass that was treated with both buffer solutions.

6. Future Considerations

The current work laid the groundwork for continued work on the glass substrate for microfluidic applications. Further characterization of the surface is required to better understand the properties of the gel layer and the method through which it is formed. The thickness of the layer should be investigated to determine the volume of the gel in order to choose a better drop volume. This will ensure that the drop is completely contained within the gel layer so that a coverplate can be attached directly to the surface. A disadvantage of the XPS technique is its insensitivity to hydrogen, which is a critical component of the gel layer. Secondary ion mass spectroscopy, or SIMS, is another characterization tool that has depth profiling strengths and can be sensitive to hydrogen and would be suitable for the measurement of the gel thickness.

When the phosphate and silicate results were compared, the effect of surface charge within the gel layer seemed to influence the electrophoresis results. It would be important to measure the surface charge on the glass to test the hypothesis using an electrokinetic analyzer. Related work would test buffer solutions of varying pH's to determine the dependence of surface charge on solution pH.

Changes to channel masking technique and geometry will also allow this technology to evolve to the next phase. The masking technique must be developed in order to pattern smaller channels. Surface geometries tested in recent literature include a two dimensional `T` and a serpentine channel. In both cases, the additional channel area increases the effective length, thus making the substrates smaller.

References

1. S. Jacobson, R. Herjenroder, A. Moore, and J.M. Ramsey, "Precolumn Reactions with Electrophoretic Analysis Integrated on a Microchip," *Anal. Chem.,* **66** [23] 4127-32 (1994).

2. V. Studer, A. Pepin, Y. Chen, and A. Ajdari, "Fabrication of Microfluidic Devices for AC Electrokinetic Fluid Pumping," *Microelectron. Eng.,* **61-62,** 915-20 (2002).

3. R.D. Rocklin, R.S. Ramsey, and J.M. Ramsey, "A Microfabricated Fluidic Device for Performing Two-Dimensional Liquid-Phase Separations," *Anal. Chem.,* **72** [21] 5244-9 (2000).

4. P.J.A. Kenis, R.F. Ismagilov, S. Takayama, and G.M. Whitesides, "Fabrication Inside Microchannels Using Fluid Flow," *Acc. Chem. Res.,* **33** [12] 841-7 (2000).

5. R. Jaeger, Modular Series on Solid State Devices, Vol. 5, *Introduction to Microelectronic Fabrication;* p. 232. Addison-Wesley, Reading, MA, 1988.

6. "Photolithography," (2003) Georgia Institute of Technology - School of Electrical and Computer Engineering. Accessed on: July 14, 2003. Available at <http://www.ece.gatech.edu/research/labs/vc/theory/photolith.html>

7. Z. Fan and D.J. Harrison, "Macromachining of Capillary Electrophoresis Injectors and Separators on Glass Chips and Evaluation of Flow at Capillary Intersections," *Anal. Chem.,* **66** [1] 177-84 (1994).

8. Z. Liang, N. Chiem, G. Ocvirk, T. Tang, K. Fluri, and D.J. Harrison, "Microfabrication of a Planar Absorbance and Fluorescence Cell for Integrated Capillary Electrophoresis Devices," *Anal. Chem.,* **68** [6] 1040-6 (1996).

9. S. Sze, *Semiconductor Devices, Physics and Technology;* p. 523. Wiley, New York, 1985.

10. J. Vossen, *Thin Film Processes;* p. 564. Academic Press, New York, 1978.

11. Y. Chen and A. Pepin, "Nanofabrication: Conventional and Nonconventional Methods," *Electrophoresis,* **22** [2] 187-207 (2001).

12. H. Becker and L.E. Locascio, "Polymer Microfluidic Devices," *Talanta,* **56** [2] 267-87 (2002).

13. L. Martynova, L. Locascio, M. Gaiten, G. Kramer, R. Christensen, and W. MacCrehan, "Fabrication of Plastic Microfluid Channels by Imprinitng Methods," *Anal. Chem.,* **69** [23] 4783-9 (1997).

14. D. Chen, F. Hsu, D. Zhan, and C. Chen, "Palladium Film Decoupler for Amperometric Detection in Electrophoresis Chips," *Anal. Chem.,* **73** [4] 758-62 (2001).

15. S. Wang, C. Perso, and M. Morris, "Effects of Alkaline Hydrolysis and Dynamic Coating on the Electroosmotic Flow in Polymeric Microfabricated Channels," *Anal. Chem.,* **72** [7] 1704-6 (2000).

16. J. Xu, L. Locascio, M. Gaiten, and C. Lee, "Room-Temperature Imprinting Method for Plastic Microchannel Fabrication," *Anal. Chem.,* **72** [8] 1930-3 (2000).

17. M. Butters, "Electrophoresis of Protein Through a Hydrated Channel"; B.S. Thesis, Alfred University, Alfred, NY, 2002.

18. N. Wead, "Novel Fabrication Method for Making Glass Microfluidic Devices"; B.S. Thesis, Alfred University, Alfred, NY, 2002.

19. J. Khandurina and A. Guttman, "Bioanalysis in Microfluidic Devices," *J. Chromatogr., A,* **943** [2] 159-83 (2002).

20. G. Lee, S. Chen, G. Huang, W. Sung, and Y. Lin, "Microfabricated Plastic Chips by Hot Embossing Methods and their Applications for DNA Separation and Detection," *Sens. Actuators, B,* **75** [1-2] 142-8 (2001).

21. Y. Liu, J. Fanguy, J. Bledsoe, and C. Henry, "Dynamic Coating using polyelectrolyte multilayers for chemical control of electroosmotic flow in capillary electrophoresis microchips," *Anal. Chem.,* **72** [24] 5939-44 (2000).

22. X. Ren, M. Bachman, G. Li, and N. Allbritton, "Electroosmotic Properties of Microfluidic Channel Composed of Poly(dimethylsiloxane)," *J. Chromatogr., B: Biomed. Sci. Appl.,* **762** [1] 117-25 (2001).

23. D.E. Clark, C.G. Pantano, Jr., and L.L. Hench, *Corrosion of Glass;* p. 75. Books for Industry, New York, 1979.

24. R. Doremus, *Glass Science*, 2nd ed. John Wiley and Sons, New York, 1994.

25. F. Wang and F. Tooley, "Detection of Reaction Products between Water and Soda-Lime-Silica Glass," *J. Amer. Ceram. Soc.,* **41** [11] 467-9 (1958).

26. F. Bacon and Calcamuggio, "Effect of Heat Treatment in Moist and Dry Atmospheres on Chemical Durability of Soda-Lime Glass Bottles," *Am. Ceram. Soc. Bull.,* **46** [9] 850-5 (1967).

27. F. Wang and F. Tooley, "Influence of Reaction Products on Reaction Between Water and Soda-Lime-Silica Glass," *J. Am. Ceram. Soc.,* **41** [12] 521-4 (1958).

28. R. Doremus, "Interdiffusion of Hydrogen and Alkali Ions in a Glass Surface," *J. Non-Cryst. Solids,* **19,** 137-44 (1975).

29. B. Bunker, D. Haaland, K. Ward, and T. Michalske, "Infrared Spectra of Edge-Shared Silicate Tetrahedra," *Surf. Sci.,* **210** [3] 406-28 (1989).

30. P.A. Schader, "Weathering Study of Fused Silica and Borosilicate Glass Surfaces"; M.S. Thesis, Alfred University, Alfred, NY, 2002.

31. B.C. Bunker, G.W. Arnold, and J.A. Wilder, "Phosphate Glass Dissolution in Aqueous Solutions," *J. Non-Cryst. Solids,* **64** [4] 291-316 (1984).

32. N.H. Ray, *Inorganic Polymers*, 1st ed.*;* p. 174. Academic Press, New York, 1978.

33. F. Vinet, P. Chaton, and Y. Fouillet, "Microarrays and Microfluidic Devices: Miniaturized Systems for Biological Analysis," *Microelectron. Eng.,* **61-62** 41-7 (2002).

34. M. Bier, *Electrophoresis: Theory, Methods, and Applications;* p. 563. Academic Press, New York, 1959.

35. R. Audubert and S. Mende, *The Principles of Electrophoresis;* p. 142. Hutchinson and Co., London, 1959.

36. J. Towns and F. Regnier, "Impact of Polycation Adsorption on Efficiency and Electroosmotically Driven Transport in Capillary Electrophoresis," *Anal. Chem.,* **64** [21] 2473-8 (1992).

37. S. Ghosal and Z. Lu, "Electroosmotic Flow and Zone Broadening in Microfluidic Channels of Variable Cross-Section and Wall Charge," (2002) Nanotech 2002,

Vol. 1, Computational Publications. Accessed on: March 31, 2004. Available at <http://www.nsti.org/procs/msm2002/2/T32.02>

38. D. Figeys and D. Pinto, "Proteomics on a Chip: Promising Developments," *Electrophoresis,* **22** [2] 208-16 (2001).

39. D. Harrison, A. Manz, Z. Fan, H. Ludi, and H. Widmer, "Capillary Electrophoresis and Sample Injection Systems Integrated on a Planar Glass Chip," *Anal. Chem.,* **64** [17] 1926-32 (1992).

40. S. Jacobson, R. Hergenroder, L. Kouty, R. Warmack, and J. Ramsey, "Effects of Injection Schemes and Column Geometry on the Performance of Microchip Electrophoresis Devices," *Anal. Chem.,* **66** [7] 1107-13 (1994).

41. D.V. McCaughan, R.A. Kushner, and V.T. Murphy, "Ion Neutralization Processes at Insulator Surfaces and Consequent Impurity Migration Effects in SiO_2 Films," *Phys. Rev. Lett.,* **30** [13] 614-7 (1973).

42. R.A. Kushner, D.V. McCaughan, V.T. Murphy, and J.A. Heilig, "Mobilization of Sodium in SiO_2 Films by Ion Bombardment," *Phys. Rev. Lett.,* **10** [6] 2632-41 (1974).

43. H. Bach, "Distortion of Sodium Concentration Profiles in Thin Glassy Surface Layers by Ion Bombardment," *Radiat. Eff.,* **28** [3-4] 215-6 (1976).

44. R.K. Brow, "Glass Surface Modifications during Ion Beam Sputtering," *J. Non-Cryst. Solids,* **107** [1] 1-10 (1988).

45. X. Zhou, P.F. Johnson, R.A. Condrate, Sr., and Y.M. Guo, "Structural Investigation of Plasma-Enhanced Surface Modification using FTIR Spectroscopy," *Mater. Lett.,* **9** [5,6] 207-10 (1990).

46. H. Watson, M. Kaunisto, J. Gustafsson, and J. Paivarinta, "The Effect of Solvent and Fiber Treatment on the Deposition of Organic Silane Solutions Using THF and Acetone," *J. Colloid Interface Sci.,* **241** [1] 32-44 (2001).

47. C. Marcott, "Infrared Spectroscopy," pp. 109-25 in Metals Handbook, 9th ed., Vol. 10, *Materials Characterization.* Edited by R.E. Whan. American Society of Metals, Metals Park, OH, 1986.

48. J.B. Lumsden, "X-Ray Photoelectron Spectroscopy," pp. 568-80 in Metals Handbook, 9th ed., Vol. 10, *Materials Characterization.* Edited by R.E. Whan. American Society for Metals, Metals Park, OH, 1986.

49. N.D. Cogger and N.J. Evans, "An Introduction to Electrochemical Impedance Measurement," Solartron Technical Report 6, 1999.

50. S. Takeda, K. Yamamoto, Y. Hayasaka, and K. Matsumoto, "Surface OH Group Governing Wettability of Commercial Glasses," *J. Non-Cryst. Solids,* **249** [1] 41-6 (1999).

51. N.K. Adam, "The Chemical Strucutre of Solid Surfaces as Deduced from Contact Angles," pp. 52-6 in Advances in Chemistry, Vol. 43, *Contact Angle: Wettability and Adhesion.* Edited by F. Fowkes. American Chemical Society, Washington, D.C., 1964.

52. R.J. Hunter, *Zeta Potential in Colloid Science;* p. 229. Academic Press, London, 1981.